

## Simulating nitrate formation mechanisms during PM<sub>2.5</sub> events in Taiwan and their implications for the controlling direction



Ming-Tung Chuang <sup>a,\*</sup>, Chang-Fu Wu <sup>b</sup>, Chuan-Yao Lin <sup>a</sup>, Wei-Che Lin <sup>a</sup>, Charles C.-K Chou <sup>a</sup>, Chung-Te Lee <sup>c</sup>, Tang-Huang Lin <sup>d</sup>, Joshua S. Fu <sup>e</sup>, Steven Soon-Kai Kong <sup>f</sup>

<sup>a</sup> Research Center for Environmental Changes, Academia Sinica, Taipei, 11529, Taiwan

<sup>b</sup> Department of Public Health, National Taiwan University, Taipei, 10055, Taiwan

<sup>c</sup> Graduate Institute of Environmental Engineering, National Central University, Taoyuan, 32001, Taiwan

<sup>d</sup> Center for Space and Remote Sensing Research, National Central University, Taoyuan, Taiwan

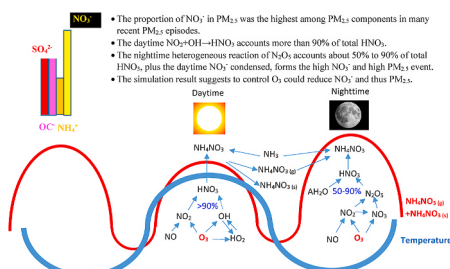
<sup>e</sup> Department of Civil and Environmental Engineering, University of Tennessee, Knoxville, TN, 37996, USA

<sup>f</sup> Department of Atmospheric Sciences, National Central University, Taoyuan, 32001, Taiwan

### HIGHLIGHTS

- The observed proportion of NO<sub>3</sub><sup>-</sup> in PM<sub>2.5</sub> has been decreasing in recent years.
- Evolution of meteorology, NO<sub>3</sub><sup>-</sup>, its precursors/intermedia products are addressed.
- The contributions of eight NO<sub>3</sub><sup>-</sup> formation pathways were calculated.
- To control O<sub>3</sub> could also reduce NO<sub>3</sub><sup>-</sup> in addition to direct NO<sub>x</sub> and NH<sub>3</sub> reduction.
- Daytime maximum O<sub>3</sub> has close relationship with daytime/nighttime maximum HNO<sub>3</sub>.

### GRAPHICAL ABSTRACT



### ARTICLE INFO

#### Keywords:

Nitrate formation mechanism

PM<sub>2.5</sub>

O<sub>3</sub>

WRF/CMAQ modeling

### ABSTRACT

The long-term downward trend of NO<sub>x</sub> concentrations does not reflect the reduction of nitrate (NO<sub>3</sub><sup>-</sup>) in Taiwan. Instead, the proportion of NO<sub>3</sub><sup>-</sup> in PM<sub>2.5</sub> increased in recent years. To probe the increasing importance of NO<sub>3</sub><sup>-</sup> in PM<sub>2.5</sub>, this study applied the WRF/CMAQ modeling system to implement a simulation from 16 March 2017 to 30 April 2017, in which 5 p.m.<sub>2.5</sub> events with daily average concentrations  $\geq 35 \mu\text{g m}^{-3}$  and their corresponding correlation coefficients (R) of simulated and observed PM<sub>2.5</sub> above 0.6 were selected for analysis. During the daytime, the reaction of NO<sub>2</sub> and OH contributed more than 90% of the total HNO<sub>3</sub>. After sunset, the high concentrations of NO<sub>3</sub> and N<sub>2</sub>O<sub>5</sub> peaked, followed soon by the simultaneous rise of NO<sub>3</sub><sup>-</sup>, aerosol water content, and HNO<sub>3</sub> concentrations around midnight, which indicated that the heterogeneous reaction was the main formation mechanism of NO<sub>3</sub><sup>-</sup>, accounting for approximately 30%–90% of total HNO<sub>3</sub>. At nighttime, the daytime-formed gaseous phase NO<sub>3</sub><sup>-</sup> condensed, and low wind and low boundary layer height favored accumulation; therefore, PM<sub>2.5</sub> peaked around the midnight period to the early morning. The sensitivity test showed that doubling and halving the NO<sub>x</sub> and NH<sub>3</sub> emissions could directly lead to the highest production and reduction of NO<sub>3</sub><sup>-</sup>, respectively, followed by doubling and halving NMHC emissions, which caused the highest and lowest O<sub>3</sub> concentrations. The correlation analysis of the simulation results showed that the daytime

\* Corresponding author. Research Center for Environmental Changes, ACADEMIA SINICA, Taipei, 11529, Taiwan. Tel.: +886-2-27875894; fax: +886-2-27833584.  
E-mail address: [mtchuang100@gmail.com](mailto:mtchuang100@gmail.com) (M.-T. Chuang).

maximum O<sub>3</sub> and HNO<sub>3</sub> were highly correlated. The relationships between daytime maximum O<sub>3</sub>, nighttime maximum NO<sub>3</sub><sup>-</sup>, N<sub>2</sub>O<sub>5</sub>, and HNO<sub>3</sub> in pairs were also moderately to highly correlated. This study implies that in addition to direct reduction of NO<sub>x</sub> or NH<sub>3</sub> emissions, controlling O<sub>3</sub> is possibly another useful strategy to reduce NO<sub>3</sub><sup>-</sup>. Because NO<sub>x</sub> emission reduction could conflict with controlling O<sub>3</sub>, this study suggests to re-examine the determination of NO<sub>x</sub>-limited and VOCs-limited regions in order to develop strategies for reducing NO<sub>x</sub> emission and O<sub>3</sub> simultaneously.

## 1. Introduction

Many epidemiological studies have shown that exposure to PM<sub>2.5</sub> (particulate matter with an aerodynamic diameter less than 2.5 μm) can harm physiological functions, can increase the risk of death, can result in delayed development, and can reduce immunity and retard growth in newborn and young children (Loftus et al., 2015). Moreover, PM<sub>2.5</sub> also absorbs and scatters solar radiation (Pani et al., 2016), harms visibility (Chen et al., 2014), affects the radiation budget and balance of the atmosphere, and changes the global climate (Wang and Chen, 2016; Song et al., 2019). Therefore, research on the formation of PM<sub>2.5</sub> is very important.

Among PM<sub>2.5</sub> species, NO<sub>3</sub><sup>-</sup> is an important species. Ge et al. (2017) discussed the formation of NO<sub>3</sub><sup>-</sup> in major cities in China (Nanjing, Beijing, and Lanzhou) and used the correlation between NO<sub>3</sub><sup>-</sup> and temperature (T), relative humidity (RH) and solar radiation to classify the formation of NO<sub>3</sub><sup>-</sup> into Type I-thermodynamics driven, Type II-photochemistry driven, and Type III-PBL (planetary boundary layer) dynamics driven. The characteristics of Type I thermodynamics are that NO<sub>3</sub><sup>-</sup> has a very good relationship with the dissociation constants (KPs) of NH<sub>4</sub>NO<sub>3</sub> and RH but a poor correlation with temperature. For Type II, NO<sub>3</sub><sup>-</sup> has a good correlation with temperature but a poor correlation with K<sub>p</sub> or RH. For Type III, the correlation between NO<sub>3</sub><sup>-</sup> and K<sub>p</sub>, RH or T is very poor. In addition, NO<sub>3</sub><sup>-</sup> in the upper atmosphere is transported downward and lifts the NO<sub>3</sub><sup>-</sup> concentration near the surface after the top of the boundary layer develops in the morning, which may be more obvious over complex terrain (Yao et al., 2014). Cheng et al. (2016) studied haze events in Beijing and found that the cause of PM<sub>2.5</sub> episodes was heterogeneous reactions on the surface of aerosols. Because the water content is high in PM<sub>2.5</sub>, the formation of NO<sub>3</sub><sup>-</sup> is a positive feedback mechanism. This mechanism can be explained by the research of Sun et al. (2018), who found that an increase in the proportion of NH<sub>4</sub>NO<sub>3</sub> in PM<sub>2.5</sub> can reduce the mutual deliquescence relative humidity (MDRH) of particles, which provides a suitable liquid shell for heterogeneous reactions when the RH is above 60%. Kuprov et al. (2009) suggested that the daytime oxidation reaction of hydroxyl radicals (OH) and NO<sub>2</sub> was the major NO<sub>3</sub><sup>-</sup> formation pathway in the Salt Lake Valley. The daytime-formed NO<sub>3</sub><sup>-</sup> could condense during nighttime. Baasandorj et al. (2017) employed measurements in winter in the Salt Lake Valley and suggested that Kuprov's findings was based on surface observations. They found N<sub>2</sub>O<sub>5</sub> converted to HNO<sub>3</sub> during the nighttime and in the early morning in the upper lever of the persistent cold-air pools. In their case study of observations, aerosol concentrations increased up to 200 m and even reached 400 m along the basin sidewall.

Air-quality modeling is a useful tool to study NO<sub>3</sub><sup>-</sup> formation mechanisms. For example, Kim et al. (2014) applied the Community Multiscale Air Quality (CMAQ, Byun and Schere, 2006) model to estimate the NO<sub>3</sub><sup>-</sup> production contributions over the Ohio River Valley and southern Greak Lakes. The total NO<sub>3</sub><sup>-</sup> in the lower troposphere was attributed to three pathways: 57% was from the heterogeneous conversion of dinitrogen pentoxide (N<sub>2</sub>O<sub>5</sub>), 28% was from the oxidation reaction of OH and NO<sub>2</sub>, and 15% was from the homogeneous conversion of N<sub>2</sub>O<sub>5</sub>. Qu et al. (2019) utilized the WRF-Chem (Weather Research and Forecasting – Chemistry, Grell et al., 2005) model to simulate the NO<sub>3</sub><sup>-</sup> formation mechanisms over the North China Plain and found that the heterogeneous hydrolysis of N<sub>2</sub>O<sub>5</sub> was the cause of high NO<sub>3</sub><sup>-</sup> in southwestern Hebei Province in China during summer, while the

photolysis of nitrous acid (HONO) produced abundant OH radicals and led to high NO<sub>3</sub><sup>-</sup> in southern Beijing and southeastern Hebei Province during winter. Kelley et al. (2021) applied a statistical fit of an efficient polynomial function in a response surface model to CMAQ simulations over the eastern U.S. for January and July 2016. Their nonlinear response showed that reduced NH<sub>3</sub> and nitrogen oxide (NO<sub>x</sub>) emissions reduced the NO<sub>3</sub><sup>-</sup> concentration in the northern U.S. In January, NH<sub>3</sub> emission reductions were more effective than NO<sub>x</sub> emission reductions. NH<sub>3</sub> emission reductions effectively reduced NO<sub>3</sub><sup>-</sup> concentrations in January but increased secondary organic aerosol concentrations in July. Sulfur dioxide (SO<sub>2</sub>) and volatile organic compounds (VOC) emission reductions have a relatively small influence on NO<sub>3</sub><sup>-</sup>, while SO<sub>2</sub> reductions might not benefit NO<sub>3</sub><sup>-</sup> in the northern U.S. Zhai et al. (2021) illustrated the nitrate component of PM<sub>2.5</sub> did not respond effectively to decreasing NO<sub>x</sub> emissions during winter haze events in the North China Plain. They applied the GEOS-Chem model (Bey et al., 2001) to reproduce the increasing NO<sub>3</sub><sup>-</sup> over 2013–2018 and suggested NH<sub>3</sub> emission reduction would be more effective than NO<sub>x</sub> or VOC emission reduction for decreasing NO<sub>3</sub><sup>-</sup>. Thunis et al. (2021) applied the EMEP air quality model (Simpson et al., 2012) to study the response of PM<sub>2.5</sub> to changes in combinations of NO<sub>x</sub> and NH<sub>3</sub> emissions in the Po Basin, Italy. Their simulation results suggest a secondary PM<sub>2.5</sub> increase when NO<sub>x</sub> emission reductions are applied in NO<sub>x</sub>-rich areas, which is caused by the increased ozone (O<sub>3</sub>).

This study simulated local PM<sub>2.5</sub> events from 16 March 2017 to 30 April 2017 to probe the formation mechanisms of NO<sub>3</sub><sup>-</sup>, estimated the contributions to HNO<sub>3</sub> from eight formation pathways, conducted sensitivity tests to examine the response of O<sub>3</sub> and PM<sub>2.5</sub> species to major gaseous emissions, and evaluated the correlation of precursors, intermediate products and the final product: HNO<sub>3</sub>. An introduction to the measurements, modeling design, regulation of modeling evaluation, and the HNO<sub>3</sub> formation pathways of the modeling is given in Section 2. The results and discussion, including the long term trend of gaseous air pollutants and PM<sub>2.5</sub> species, modeling performance, temporal evolution of NO<sub>3</sub><sup>-</sup> and related species in PM<sub>2.5</sub> events, contributions of HNO<sub>3</sub> formation pathways, and the relationship of HNO<sub>3</sub> and its precursors or intermediate products, are provided in Section 3, and the conclusion is presented in Section 4.

## 2. Research methods

### 2.1. Description of automatic air quality monitoring and manual sampling for long-term trend analysis

A long-term (2003–2020) trend of gaseous precursors, O<sub>3</sub>, and PM<sub>2.5</sub> was based on data collected from representative air quality sites in western Taiwan (indicated by the green triangles in Fig. 1): Banqiao (BQ in Fig. 1), Zhongming (ZM in Fig. 1), Tainan (TN in Fig. 1), and Xiaogang (XG in Fig. 1). According to the Taiwan Environmental Protection Agency (TWEPA) announcement, SO<sub>2</sub>, NO<sub>x</sub>, O<sub>3</sub> and nonmethane hydrocarbon (NMHC) were automatically measured with an Ecotech 9850 (Ecotech Monitoring Solution PVT, Ltd), an Ecotech 9841, an Ecotech 9810, and a Horiba-APHA 360 (Horiba, Ltd), respectively. PM<sub>2.5</sub> was measured with a Met-One BAM-1020 (Met One Instruments, Inc.) at BQ, ZM, and TN and with a VEREWA-F701 (DURAG GROUP) at XG. In addition, NH<sub>3</sub> was measured with a Serinus-44 (Ecotech Monitoring Solution PVT, Ltd) at Xinzhuang (XZ in Fig. 1), Lunbei (LB in Fig. 1),

Chenzhen (CZ in Fig. 1), and Daliao (DaL in Fig. 1). The above air quality sites are routinely maintained by the Taiwan Environmental Protection Agency.

In addition to automatic monitoring, this study also displayed the PM<sub>2.5</sub> species of manually collected samples for two sampling periods. Sampling period I was from 2003 to 2009 (Chou et al., 2008, 2010) at 7 p.m. sampling sites (indicated by the yellow stars in Fig. 1): National Taiwan University (NTU in Fig. 1); National Chung Hsing University (NCHU in Fig. 1); TN and Pingtung (PT in Fig. 1). For sampling period II from 2015 to 2019, Lee et al. (2020) sampled PM<sub>2.5</sub> at BQ, ZM, Douliu (DL in Fig. 1), Chiayi (CY in Fig. 1), XG, and HL, which are all indicated as crosses in white circles in Fig. 1. MG and HL can be considered country sites located in the middle of the Taiwan Strait and on the eastern coast of Taiwan, respectively, and they are mainly influenced by the background oceanic atmosphere. NTU, BQ, NCHU, ZM, CY, TN, and XG can be considered urban sites because they are located in densely populated areas with hundreds of thousands to millions of people and where mobile and anthropogenic/business activities are the main sources. XG is a special site because it is located in Kaohsiung city near the Kaohsiung harbor and influenced by many industrial parks in the neighborhood. PT and DL can be considered rural sites because they are located in small cities where tens of thousands of people live, and surrounding agriculture is the main economic activity contributing to pollution along with urban automobile sources.

For sampling period I, the PM<sub>2.5</sub> samples were collected with PTFE membrane filters and analyzed for water soluble ions, such as sodium ions ( $\text{Na}^+$ ), potassium ions ( $\text{K}^+$ ),  $\text{NH}_4^+$ , calcium ions ( $\text{Ca}^{2+}$ ), magnesium ions ( $\text{Mg}^{2+}$ ), chlorine ions ( $\text{Cl}^-$ ),  $\text{NO}_3^-$ , and  $\text{SO}_4^{2-}$ , by ion chromatography (IC, Dionex DX100) and OC/EC (organic carbon/elemental carbon) by a DRI-2001A carbonaceous aerosol analyzer, following the Interagency Monitoring of PROtected Visual Environments (IMPROVE) thermo-optical reflectance (TOR) protocol (Chow et al., 2001). The sampling and analytical methods can be found in Chou et al. (2008, 2010). In the first three years, the sampling was randomly conducted several times a month but later fixed on the last week of each month. Due to rain, sampling device malfunctions, and sample analysis accidents, the numbers of sampling data were different for each site, as indicated in Table 1.

For sampling period II, the PM<sub>2.5</sub> sampling frequency was every six days, and each sample was collected for 24 h (00:00 LST–24:00 LST, Lee

et al., 2020). The samples for mass weighing were collected with a MetOne E-FRM sampler (Met One Instruments, Inc.), which complies with the U.S. EPA certification RFPS-0315-221. Samples for chemical analysis were collected with MetOne SASS PM<sub>2.5</sub> samplers, which are also used in the U.S. Chemical Speciation Network (CSN). The Teflon and quartz filters in the samplers were used for water soluble ions and carbon analysis, respectively. For manual sampling, unless Chou et al. (2008) and Lee et al. (2020) found any mistakes in the analytical process, all data were reserved for further analysis.

## 2.2. Modeling design

During the crossover between the southwestern and northeastern monsoon seasons, e.g., April and May and September and October, respectively, the PM<sub>2.5</sub> level is usually high due to local pollution (Chuang et al., 2008). This study used the WRF/CMAQ model to simulate the PM<sub>2.5</sub> episodes from 16 March 2017 to 30 April 2017. Two classical local PM<sub>2.5</sub> events occurring at the CY and DL sites on approximately 19 and 25 April 2017, respectively, were selected for detailed analysis. In addition, 7 p.m. sampling samples were collected on 20 and 26 March, and 1, 7, 13, 19, and 25 April 2017 were chosen to analyze the attribution of  $\text{NO}_3^-$  formation pathways. Sensitivity tests of the response of  $\text{O}_3$ ,  $\text{NO}_3^-$ ,  $\text{SO}_4^{2-}$ , OC, and  $\text{NH}_4^+$  to the change in precursors and the correlation of  $\text{HNO}_3$  and its precursors and intermediate products were implemented. The WRF/CMAQ modeling system consisted of the WRF (Skamarock et al., 2008) meteorological model and CMAQ chemical transport model. The model versions for WRF and CMAQ used in this study were 3.9.1 and 5.2.1, respectively.

The simulation was designed as two nested domains with horizontal resolutions of 9 and 3 km, as illustrated in the left subfigure in Fig. 1. The first domain covered East Asia, and the second covered Taiwan, part of the Asian continent (Fujian Province) and surrounding waters. The vertical layers contained 45 layers with 24 layers below 3000 m and 16 layers below 1000 m, specifically, 0, 25, 50, 75, 100, 135, 180, 230, 290, 360, 440, 525, 625, 730, 850, and 1000 m over water (not fixed values, which may change due to temperature and pressure). Therefore, the vertical resolution should have well resolved the boundary layer.

The initial meteorological field for WRF modeling was from NCEP GFS (National Centers for Environmental Prediction, Global Forecast System) reanalysis data with a horizontal resolution of  $0.25^\circ \times 0.25^\circ$ .

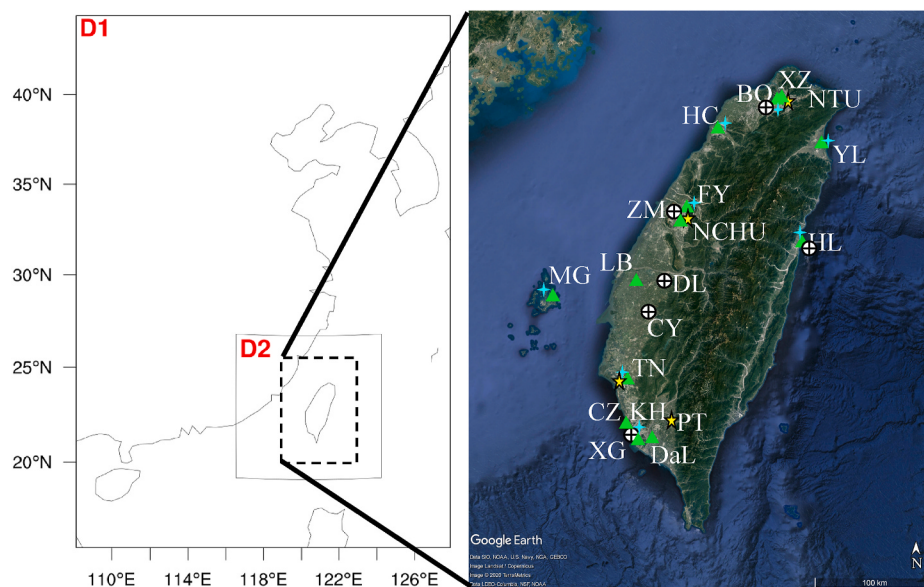


**Fig. 1.** Domains of simulation range (left) and geographic locations of Taiwan CWB (Central Weather Bureau) meteorological sites (●): BQ, HC, FY, TN, KH, YL, HL, and MG; TWEPA (Taiwan Environmental Protection Agency) air quality monitoring sites (▲): BQ, HC, FY, TN, XG, YL, HL, MG, ZM, XZ, LB, CZ, Dal; PM<sub>2.5</sub> sampling sites for sampling period I (★): NTU, NCHU, TN, and PT; and PM<sub>2.5</sub> sampling sites for sampling period II (⊕): BQ, ZM, DL, CY, XG, and HL (right).

**Table 1**

p.m.<sub>2.5</sub> and their respective PM<sub>2.5</sub> species concentrations for PM<sub>2.5</sub> episodes in which the daily PM<sub>2.5</sub> conc.  $\geq 35 \mu\text{g m}^{-3}$  on sampling days during sampling period I and II.

Sampling period	Site	No. of samples	PM <sub>2.5</sub>	SO <sub>4</sub> <sup>2-</sup>	NO <sub>3</sub> <sup>-</sup>	NH <sub>4</sub> <sup>+</sup>	K <sup>+</sup> +Mg <sup>2+</sup> +Ca <sup>2+</sup>	Na <sup>+</sup> +Cl <sup>-</sup>	OC	EC	Others
I 2003   2009	CFG	96	45.8 ± 9.5	14.6 ± 5.3	1.5 ± 1.5	4.4 ± 1.8	1.0 ± 0.6	1.4 ± 1.3	6.0 ± 1.9	1.9 ± 0.8	15.8 ± 6.9
	NTU	116	50.2 ± 12.5	12.0 ± 4.7	3.1 ± 2.3	5.0 ± 1.9	0.7 ± 0.5	0.4 ± 0.4	7.5 ± 2.3	3.1 ± 1.2	18.7 ± 7.4
	NCHU	174	56.1 ± 22.6	11.5 ± 5.6	5.6 ± 4.7	6.0 ± 3.3	0.9 ± 0.5	1.2 ± 1.0	10.4 ± 5.2	3.9 ± 1.8	16.8 ± 12.5
	TN	63	60.0 ± 15.6	12.1 ± 4.7	7.5 ± 5.0	6.5 ± 2.4	1.1 ± 0.9	1.2 ± 1.1	9.1 ± 2.7	3.2 ± 0.9	19.9 ± 9.9
	PT	147	57.4 ± 16.0	10.1 ± 3.9	6.9 ± 4.6	5.7 ± 2.2	1.0 ± 0.5	1.4 ± 1.0	10.0 ± 3.1	2.4 ± 1.0	20.0 ± 9.0
	HL	37	45.5 ± 7.7	14.9 ± 3.7	1.2 ± 0.8	5.2 ± 1.4	1.7 ± 1.2	0.8 ± 0.9	6.5 ± 2.2	2.3 ± 0.8	12.9 ± 5.7
II 2015   2019	MG	61	46.6 ± 36.6	9.9 ± 4.0	1.1 ± 1.4	2.9 ± 1.8	1.8 ± 1.3	2.4 ± 1.8	3.8 ± 2.0	1.6 ± 0.6	18.9 ± 8.8
	BQ	20	43.7 ± 12.9	10.3 ± 3.8	5.5 ± 4.0	4.9 ± 2.1	0.4 ± 0.3	0.7 ± 0.5	7.5 ± 2.1	1.9 ± 0.6	12.3 ± 5.2
	ZM	41	47.2 ± 12.8	9.7 ± 2.9	8.9 ± 4.0	5.6 ± 1.3	0.4 ± 0.2	1.2 ± 0.7	7.6 ± 2.2	1.9 ± 1.7	11.9 ± 5.3
	DL	59	46.7 ± 9.4	7.6 ± 2.5	9.9 ± 4.5	5.2 ± 1.6	0.5 ± 0.2	1.5 ± 0.7	8.4 ± 2.0	1.7 ± 0.5	12.1 ± 4.6
	CY	56	49.0 ± 11.1	7.9 ± 2.4	11.6 ± 4.6	5.8 ± 1.6	0.5 ± 0.3	1.8 ± 0.8	7.7 ± 1.7	1.7 ± 0.7	12.1 ± 5.0
	XG	67	47.0 ± 10.5	7.8 ± 2.9	11.2 ± 3.7	5.5 ± 1.3	0.4 ± 0.2	1.4 ± 0.6	7.7 ± 1.6	2.0 ± 0.9	11.0 ± 4.4

Note: unit of PM<sub>2.5</sub> conc. is  $\mu\text{g m}^{-3}$ ; values for PM<sub>2.5</sub> components are the percentage of total PM<sub>2.5</sub>; data of sampling I is from Chou et al. (2008) who collected samples at the last week of each month from 2003 to 2009; data of sampling period II is from Lee et al. (2020) who collected samples every six days from 2015 to 2019; “Others” means unresolved components.

Moreover, four-dimensional data assimilation with grid and observation nudging was applied for the first and second domains, respectively, to obtain better meteorological modeling output. The anthropogenic emissions for the Asian region (outside Taiwan) and Taiwan Island were from MIX v1.1 (Multiresolution Emission Inventory for China version 1.1, Li et al., 2017) and TEDS 10.0 (Taiwan Emission Data System version 10.0, TWEPA, 2017), which were based on 2010 and 2016, respectively. The MIX emissions of SO<sub>2</sub>, NO<sub>x</sub>, NMHC, NH<sub>3</sub>, CO, PM<sub>10</sub>, and PM<sub>2.5</sub> covering the Chinese mainland were adjusted with changes of -62%, -17%, 11%, 1%, -27%, -38%, and -35%, respectively, according to the annual changes between 2010 and 2017 (Zheng et al., 2018). For other regions except the Chinese mainland and Taiwan, anthropogenic emissions remained unchanged. The biogenic emissions for Asian regions (outside Taiwan) and Taiwan were from MEGAN v2.10 (Model of Emissions of Gases and Aerosols from Nature version 2.10, Guenther et al., 2012) and BEIS v3.61 (Biogenic Emission Inventory System version 3.61, Vukovich and Pierce, 2002), respectively. The latter was used because we collected the relatively complete vegetation distribution database in Taiwan and applied the SMOKE v4.6 (Sparse Matrix Operator Kernel Emissions version 4.6, Houyoux and Vukovich, 1999) emission system. The modeling configuration was the same as that of Chuang et al. (2017) and can be found in Supplement Table S1.

### 2.3. Evaluation of modeling

The evaluation of air quality modeling results has three parts: meteorological modeling, general air pollutants of air quality modeling, and PM<sub>2.5</sub> species of air quality modeling. The formulas for the statistical evaluation indices are listed in Supplement Table S2.

For meteorological modeling evaluation, the present study chose sites in BQ, HC, FY, TN, Kaohsing (KH in Fig. 1), Ylian (YL in Fig. 1), Hualien (HL in Fig. 1), and MG (blue crosses in Fig. 1) to evaluate surface temperature, wind direction, wind speed, and RH. The Propeller Wind Direction Anemometer (Komatsu's Geophysical Instruments), Isuzu Seisakusho 3–3122 Quartz Precision Thermo-Hygrograph (Isuzu Seisakusho Co., Ltd.), and R.M. Young 05103 Pt-Electrical Resistance Thermometer (R.M. Young Company) were used to monitor the wind speed/direction, relative humidity and air temperature, respectively. The measurement equipment was under routine calibration by the Taiwan CWB (Central Weather Bureau, <https://www.cwb.gov.tw/Data/knowledge/announce/MIC.pdf>). These observations were evaluated with indices such as the mean bias (MB), mean average gross error (MAGE), root mean square error (RMSE), wind normalized mean bias (WNMB), and wind normalized mean error (WNME).

For the evaluation of general pollutants of air quality modeling, we also chose the BQ, HC, FY, TN, XG, YL, HL, and MG sites (green triangles

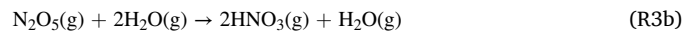
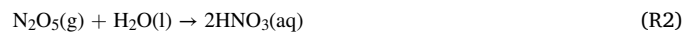
in Fig. 1), where the PM<sub>2.5</sub>, SO<sub>2</sub>, NO<sub>2</sub>, and NMHC were evaluated with the mean fractional bias (MFB), mean fractional error (MFE), R, and index of agreement (IOA). The measurement instruments of the air pollutants installed at the above sites were the same as those described in Section 2.1.

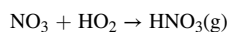
For the evaluation of PM<sub>2.5</sub> species of air quality modeling, observations came from six manual sampling sites: BQ, ZM, DL, CY, XG, and HL (crosses in white circles in Fig. 1), which were collected and analyzed by Lee et al. (2020). For each site, only 7 p.m.<sub>2.5</sub> samples were collected from 16 March 2017 to 30 April 2017, i.e., 20 and 26 March and 1, 7, 13, 19, and 25 April 2017. Metrics such as R, NMB, and NME were used for evaluation.

All statistical evaluation indices mentioned above were based on the “air quality simulation norm” regulated by the TWEPA (2016), except for the IOA, which was from Emery et al. (2001). The meteorological modeling results for the entire simulation period were evaluated. However, since the first ten days were considered the spin-up of the chemical simulation, only the CMAQ modeling results from 26 March 2017 to 30 April 2017 were evaluated. For PM<sub>2.5</sub> species of air quality modeling, we only compared PM<sub>2.5</sub> samples observed at the aforementioned six sampling sites on the seven days with simulated PM<sub>2.5</sub> species.

### 2.4. Formation pathways and rate of change of HNO<sub>3</sub>

We used the integrated reaction rate (IRR) tool in CMAQ to estimate the rate of change of HNO<sub>3</sub> that was attributed to eight pathways in the cb05e51\_ae6\_aq mechanism of CMAQv5.2.1. The rate of change of HNO<sub>3</sub> was estimated from eight formation pathways: oxidation reaction of OH and NO<sub>2</sub> (R1), nighttime heterogeneous reaction of N<sub>2</sub>O<sub>5</sub> (R2), nighttime homogeneous reaction of N<sub>2</sub>O<sub>5</sub> (R3a, R3b), reaction of hydrocarbons and NO<sub>3</sub> radicals (R4), reduction reaction of organic nitrate (R5), reaction of NO and HO<sub>2</sub> radicals (R6), reaction of NO<sub>3</sub> and HO<sub>2</sub> radicals (R7), and heterogeneous reaction of NO<sub>2</sub> on the surface of aerosols (R8). The chemical equations for these eight formation pathways are written as follows:





### 3. Results and discussion

#### 3.1. Evaluation of meteorological and air quality modeling results

The goal of this study is to study the  $\text{NO}_3^-$  formation mechanisms and to attempt to determine how  $\text{NO}_3^-$  is formed during  $\text{PM}_{2.5}$  events by applying air quality modeling. Evaluating the performance of the simulation results is an important step before further analysis. As mentioned in Section 2.3, the model evaluation includes three parts: meteorological modeling, general air pollutants of air quality modeling, and  $\text{PM}_{2.5}$  species of air quality modeling.

From Supplement Table S3, the evaluation of meteorological modeling shows that the surface temperature performed well. Even though the temperature at the KH site was slightly underestimated, probably because it was located near the seashore and influenced by sea water, it still complied with the benchmark (Supplement Fig. S1). For wind speed, the modeling results were slightly overestimated at the MG site, possibly because it was in the middle of the Taiwan Strait, where there is a strong tunnel effect between mountains in Taiwan and Fujian (the province across the Taiwan Strait facing Taiwan), but all other sites on Taiwan Island performed well (Fig. S2). The simulated wind direction performed well at all sites (Fig. S3). Although there was no benchmark for relative humidity, the bias and error of this modeling item for all sites were very small (Fig. S4).

The chemical modeling performance showed that  $\text{PM}_{2.5}$  was slightly underestimated at the HL and MG sites (Table S4, Fig. S5). The underestimation for these two sites could have been due to overestimated wind speed, uncertainty of emissions, and possibly underestimation of background concentrations. For  $\text{SO}_2$  (Fig. S6), the bias and error performed well except for MG, but the R values were not sufficiently high for all sites because both the simulated and observed values were low and concentrated in scatter plots such that good regression lines were not easily satisfied. The simulated  $\text{NO}_2$  was slightly underestimated at the XG and MG sites and overestimated at the YL and HL sites but was basically acceptable (Fig. S7). For NMHC, R values were good for all sites except for FY, which could have been due to the trend of NMHC emissions around FY in the simulation being far from reality. The underestimation of the simulated NMHC at XG (Fig. S8) was possibly related to the uncertainty of emissions in Kaohsiung Harbor.

From 16 March 2017 to 30 April 2017, there were 7 p.m. samples for each of the six sites: BQ, ZM, DL, CY, XG, and HL. Although the simulations for 20 March and 27 March were within the spin-up of the simulation from 16 March to 26 March, these two days were also included for evaluations of  $\text{PM}_{2.5}$  species to increase the amount of data for the representativeness of statistical evaluation. The comparison of observed and simulated  $\text{PM}_{2.5}$  species is shown in Fig. 2. Obviously, the simulations were more or less underestimated or overestimated due to uncertainty in emissions or in the meteorological or chemical simulations. Most discrepancies occurred at DL and CY on 13 April 2017. The severe underestimation of simulated  $\text{PM}_{2.5}$  at these two sites on that day was due to overestimated rainfall (Fig. S9). The scatter plots of simulated and observed  $\text{PM}_{2.5}$  and  $\text{PM}_{2.5}$  species are shown in Fig. S10. For most points, the simulated  $\text{SO}_4^{2-}$ , OC,  $\text{Na}^+ + \text{Cl}^-$ , and  $\text{K}^+ + \text{Mg}^{2+} + \text{Ca}^{2+}$  were underestimated. The remaining  $\text{PM}_{2.5}$  species were simulated well, but obviously, there were still a few significant discrepancies, which were due to the uncertainty of emission inventory or meteorological or chemical modeling. Compared with the benchmarks recommended by Emery et al. (2017) and Huang et al. (2021), the performance of metrics met almost all criteria standards, as indicated in Table S5.

#### 3.2. The long-term trend of gaseous pollutants and $\text{PM}_{2.5}$ species

The long-term trends of  $\text{PM}_{2.5}$  and gaseous pollutants monitored at four representative air quality sites over western Taiwan are illustrated in Fig. 3. It is obvious that  $\text{PM}_{2.5}$ ,  $\text{SO}_2$ ,  $\text{NO}_x$ , and NMHC showed downtrends from 2003 to 2020.  $\text{NH}_3$  decreased annually at XZ, CZ, and DaL but increased at LB.  $\text{O}_3$  remained approximately at the mean level in the long term. It seems that the reduction in  $\text{NO}_x$  and NMHC did not result in the expected decrease in  $\text{O}_3$  concentrations.

For the long-term trend analysis of  $\text{PM}_{2.5}$  species, we combined the data of manual  $\text{PM}_{2.5}$  samples collected for two sampling periods described in Section 2.1. For example, the  $\text{PM}_{2.5}$  species at the NTU and BQ sites in Taipei city were linked to represent the long-term trend of  $\text{PM}_{2.5}$  species in northern Taiwan. Similarly, we combined the  $\text{PM}_{2.5}$  species at the NCHU and ZM sites in central Taiwan, TN and CY sites in southwestern Taiwan and PT and XG sites in southern Taiwan to present the long-term trend in separate regions.

The long-term trend of the proportion of  $\text{PM}_{2.5}$  species in  $\text{PM}_{2.5}$  from sampling period I: 2005–2009 (Chou et al., 2008, 2010) and sampling period II: 2015–2019 (Lee et al., 2020) are illustrated in Fig. 4. Note that there was a temporal gap between these two sampling periods; therefore, the trend is not continuous in the subfigures of Fig. 3. For all  $\text{PM}_{2.5}$  episodes (daily  $\text{PM}_{2.5}$  conc.  $\geq 35 \mu\text{g m}^{-3}$ ) recorded in Chou et al. (2008, 2010), i.e., during sampling period I,  $\text{SO}_4^{2-}$  was the highest among the  $\text{PM}_{2.5}$  species, followed by OC and  $\text{NH}_4^+$  (Table 1). However, in recent years, during sampling period II,  $\text{NO}_3^-$  has become the major  $\text{PM}_{2.5}$  species during  $\text{PM}_{2.5}$  episodes, especially in southwestern and southern Taiwan. Obviously, the long-term trend of the proportion of  $\text{NO}_3^-$  in  $\text{PM}_{2.5}$  was increasing at all sampling sites in western Taiwan. Similar to  $\text{O}_3$ , the downward trend of  $\text{NO}_x$  concentration was also not consistent with the trend of  $\text{NO}_3^-$ .

#### 3.3. Temporal evolution of meteorology, $\text{NO}_3^-$ and its related precursors and intermediate products during classical $\text{PM}_{2.5}$ events

In the following section, we intended to simulate the temporal evolution of the  $\text{NO}_3^-$  formation process. However, hourly measurements of  $\text{PM}_{2.5}$  species were lacking in this study. Thus, we conservatively analyzed well-simulated  $\text{PM}_{2.5}$  events for this study. First, we selected  $\text{PM}_{2.5}$  events with daily average concentrations  $\geq 35 \mu\text{g m}^{-3}$  (Table S6). Second, we calculated the R of 72 pairs of hourly observed and simulated  $\text{PM}_{2.5}$  concentrations from the day before the sampling day to the day after (Table S7). Then, we determined the qualified  $\text{PM}_{2.5}$  events of daily average concentration  $\geq 35 \mu\text{g m}^{-3}$  and their corresponding R values were above 0.6: at the CY site on 1 April, at the ZM and DL sites on April 19, and at the BQ and CY sites on 25 April for the analysis of  $\text{NO}_3^-$  formation. Among these 5 p.m. events, we selected two occurring at CY on 25 April 2017 and at DL on 19 April 2017 because observed high  $\text{NO}_3^-$  concentrations were recorded at these two events during the simulation period for discussing the temporal evolution of  $\text{NO}_3^-$  and related species. The days before and after the sampling day were also included for discussion. It is noted that the hourly  $\text{PM}_{2.5}$  species,  $\text{HNO}_3$ ,  $\text{OH}$ , nitrate radical ( $\text{NO}_3$ ), peroxy radical ( $\text{HO}_2$ ),  $\text{N}_2\text{O}_5$ , HONO, aerosol water content (the following is represented by  $\text{AH}_2\text{O}$ ), peroxyacetyl nitrate (PAN), C3 and higher peroxyacetyl nitrate (PAN<sub>x</sub>), lumped alkyl nitrate (NTR), and peroxy nitric acid (PNA,  $\text{HNO}_4$ ), were from simulation results without verification of observations.

##### 3.3.1. $\text{PM}_{2.5}$ events occurring at CY on approximately 25 April 2017

On 24 April, an anticyclone moved to Japan from the Asian continent. Peripheral circulation prevailed eastward in eastern Taiwan (Fig. S11a). On 25 April 2017, the aforementioned anticyclone moved further eastward, and its peripheral circulation prevailed southeastern wind around Taiwan (Fig. S11b). The high mountains in Taiwan blocked the prevailing eastern or southeastern wind; therefore, calm wind formed on the leeward side of the mountains, i.e., western Taiwan. The

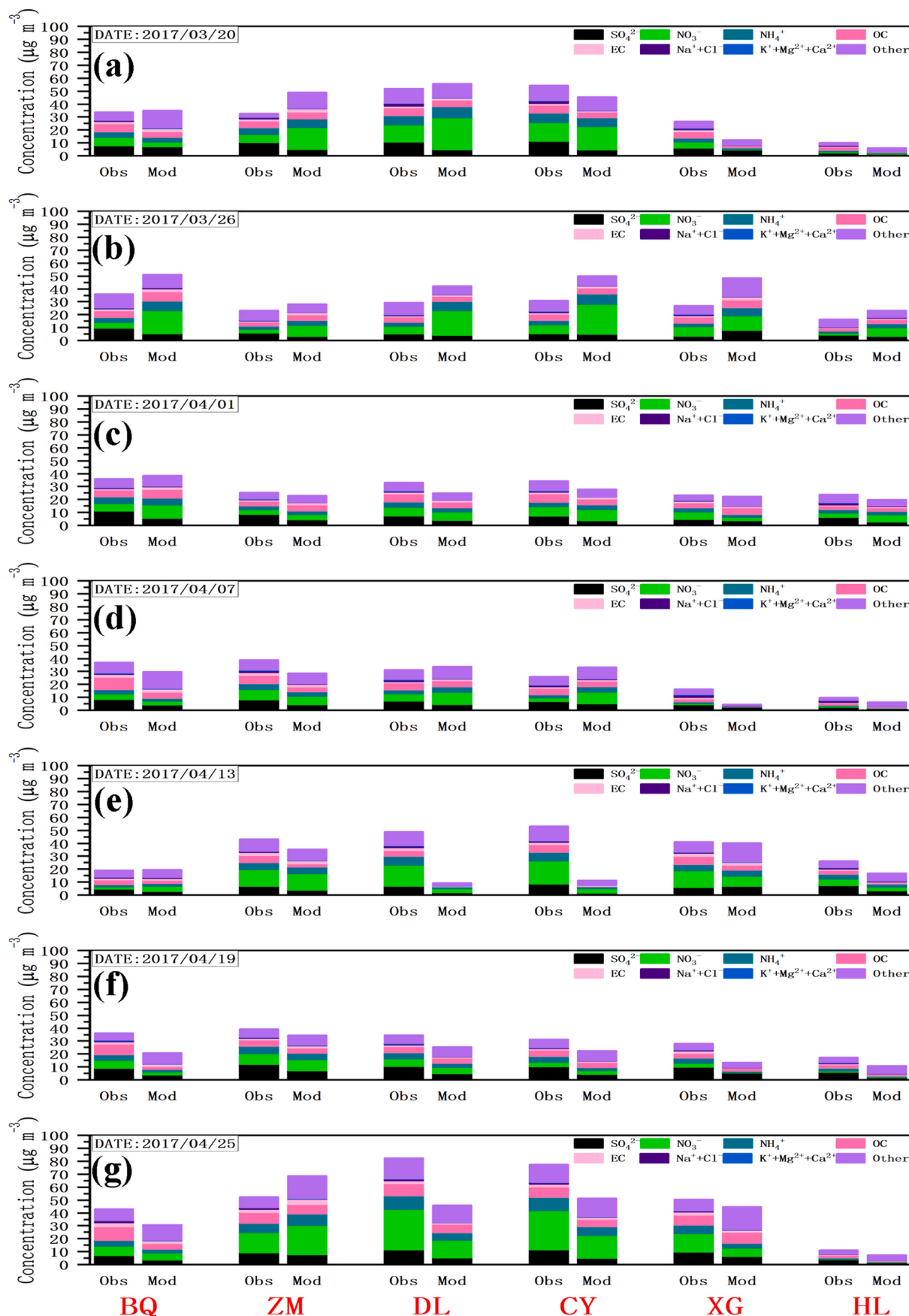


**Fig. 2.** The manually observed and modeled PM<sub>2.5</sub> species at six sampling sites (BQ/ZM/DL/CY/XG/XL) on seven sampling days: (a) 20 March (b) 26 March (c) 1 April (d) 7 April (e) 13 April (f) 19 April (g) 25 April 2017.

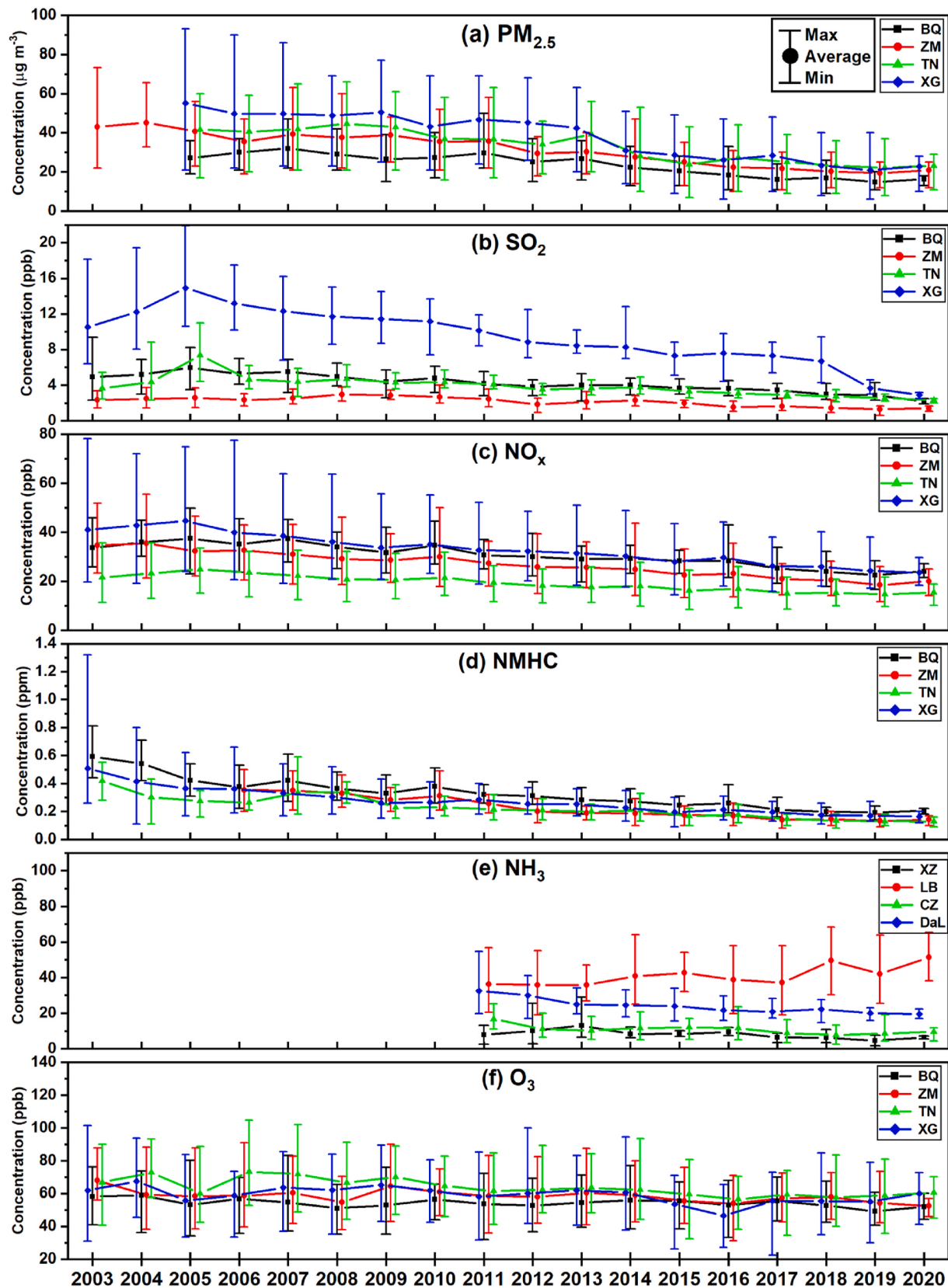


**Fig. 3.** The long-term trend of annual concentrations for (a)  $\text{PM}_{2.5}$  (b)  $\text{SO}_2$  (c)  $\text{NO}_x$  (d) NMHC (e)  $\text{NH}_3$  (f)  $\text{O}_3$  from 2003 to 2020; the three short horizontal whiskers on the line symbols represent annual maximum, annual average, and annual minimum of the corresponding monthly averages in each year. For (a)–(e), the monthly average is calculated by the average of daily average in each month, but for (f)  $\text{O}_3$ , the monthly average is calculated by the average of daily maximum in each month.

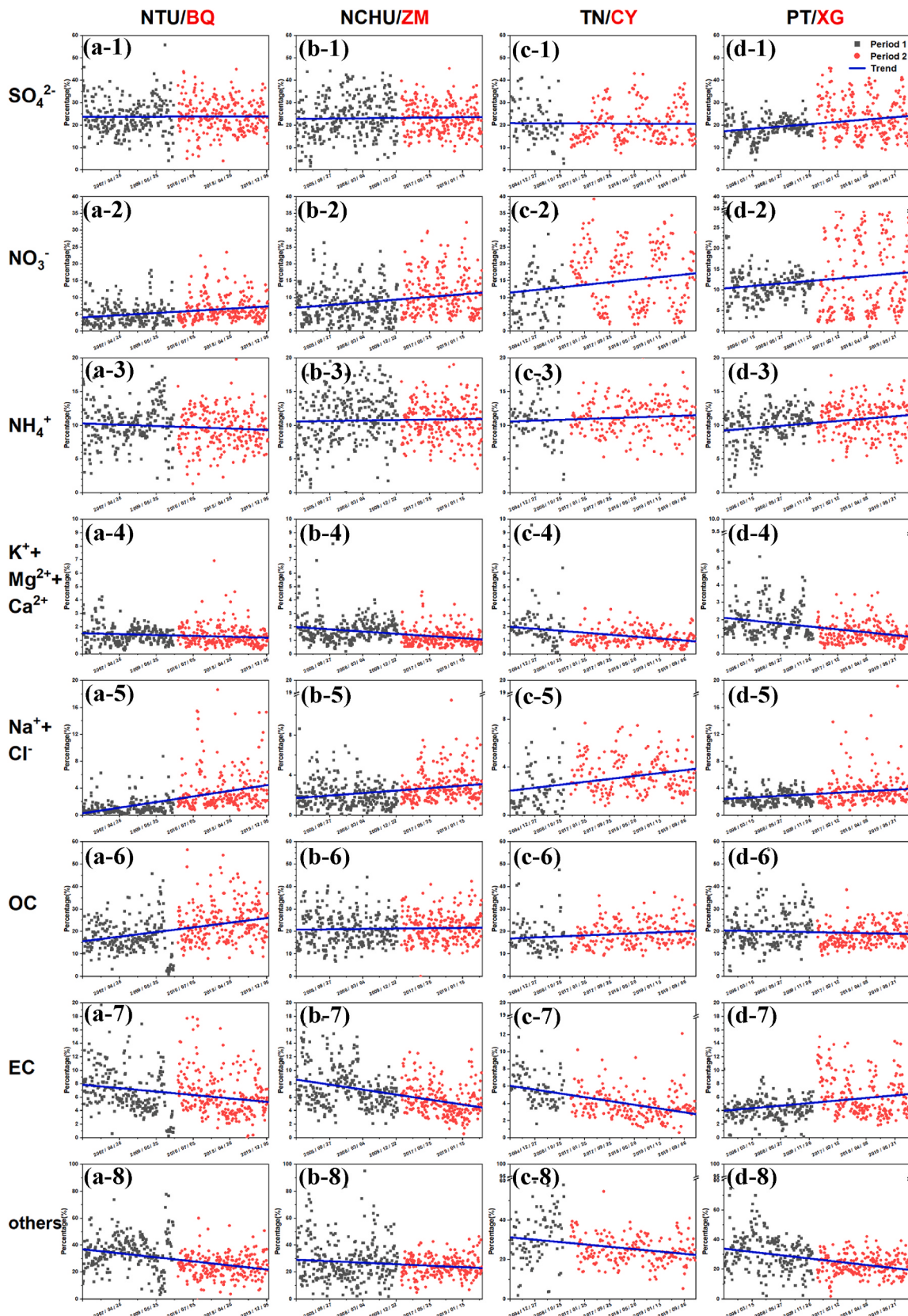


**Fig. 4.** The long-term trend of proportion of PM<sub>2.5</sub> species: (1) SO<sub>4</sub><sup>2-</sup> (2) NO<sub>3</sub><sup>-</sup> (3) NH<sub>4</sub><sup>+</sup> (4) K<sup>+</sup>+Mg<sup>2+</sup>+Ca<sup>2+</sup> (5) Na<sup>+</sup>+Cl<sup>-</sup> (6) OC (7) EC (8) others in PM<sub>2.5</sub> at (a) NCU/BQ (b) NCHU/ZM (c) TN/CY (d) PT/XG sites for sampling period I (2005–2009, black dots) and sampling period II (2015–2019, red dots). The regression lines are drawn in blue. (For interpretation of the references to colour in this figure legend, the reader is referred to the Web version of this article.)

calm wind environment favored the accumulation of PM<sub>2.5</sub>, which was reproduced well by the simulation (Fig. S12a–S12j). On 26 April 2017, an anticyclone over the Asian continent moved southeastward. Northern and northeastern winds prevailed over Korea, the coast of mainland China, the East China Sea, Taiwan, and the northern South China Sea (Fig. S11c). The strong wind quickly diluted the accumulated PM<sub>2.5</sub> in Taiwan (Fig. S12k–S12l).

From Fig. 5a–e, it is obvious that the near-surface simulated wind speed, wind direction, temperature, and RH were very close to the observations. The calm wind and low PBLH (planetary boundary layer height) around the midnight period both favored the accumulation of PM<sub>2.5</sub> (Fig. 5a and f). Although a simulated PBLH of approximately 80 m around the midnight period was unidentified because there was no measurement for this event, the PBLH below 80 m had already been recorded in many places in Taiwan (Chang et al., 2006; Ho, 2015). The CY site was located on the Jianan Plain (southwestern Taiwan), where a low PBLH occurred in a clear sky during nighttime period due to radiative cooling.

The simulated PM<sub>2.5</sub> caught the daily maximum at 00:00 25 April and 00:00 26 April well but was underestimated for the remaining time (Fig. 5f). The near-zero concentration that occurred on 16:00 on 25 April was due to unexpected simulated rainfall (Fig. 5d; actually, there was no rainfall at that time on record). The simulated PM<sub>2.5</sub> reached 92  $\mu\text{g m}^{-3}$  at 01:00 on 25 April and 96  $\mu\text{g m}^{-3}$  at 00:00 on 26 April (Fig. 5f, the actual observed PM<sub>2.5</sub> was 98  $\mu\text{g m}^{-3}$  at 00:00 and 101  $\mu\text{g m}^{-3}$  at 07:00 on 25 April and 89  $\mu\text{g m}^{-3}$  at 00:00 on 26 April). The simulated O<sub>3</sub> was slightly overestimated from the afternoon of 25 April to the early morning of 26 April but was close to the observations for the remaining time (Fig. 5g). The simulated O<sub>3</sub> concentrations were 94 ppb at 12:00 on 24 April and 107 ppb at 13:00 on 25 April (actual O<sub>3</sub> was 70 ppb at 12:00 on 24 April and 86 ppb at 12:00 on 25 April). Simulated NO and NO<sub>2</sub> performed well but occasionally overestimated (Fig. 5h and i). In contrast, simulated SO<sub>2</sub> was frequently underestimated (Fig. 5j).

Fig. 5l shows that the proportion of NO<sub>3</sub><sup>-</sup> in PM<sub>2.5</sub> was highest among PM<sub>2.5</sub> species at night. NO<sub>3</sub><sup>-</sup> contributed the most to PM<sub>2.5</sub> and synchronously changed with PM<sub>2.5</sub>. O<sub>3</sub> changed synchronously with OH and HNO<sub>3</sub> (Fig. 5m). The daytime-produced O<sub>3</sub> oxidized NO<sub>2</sub> and produced NO<sub>3</sub>, which subsequently formed N<sub>2</sub>O<sub>5</sub> at night (Fig. 5n). AH<sub>2</sub>O, NO<sub>3</sub><sup>-</sup>, and HONO synchronously peaked at midnight, which indicates that heterogeneous reactions were the main formation mechanism of NO<sub>3</sub><sup>-</sup> (Fig. 5o). Small amounts of peroxy-oxidized nitrates, such as NTR, PNA, PAN, and PANX, peaked at both noon and midnight.

### 3.3.2. PM<sub>2.5</sub> events occurring at DL on approximately 19 April 2017

In the morning of 18 April 2017, a cold front passed Taiwan, but the anticyclone over the Asian continent did not follow closely (Fig. S13a). Soon, the anticyclone moved quickly to the East China Sea on 19 April (Fig. S13b). The peripheral circulation of the anticyclone prevailed southeastern wind in eastern Taiwan. Due to mountains blocking the prevailing wind, the low wind condition on the leeward side was favorable for PM<sub>2.5</sub> accumulation (Figs. S14d–S14f). On the next day, a cold front formed from the East China Sea to southern China. Taiwan was located in the warm area ahead of the cold front (Fig. S13c). However, the observed temperature during the daytime on 20 April was slightly lower than that on 19 April (Fig. 6c), which explains some of the cold air from the Asian continent had already crossed the cold front and arrived at Taiwan. The mix of cold and warm conditions could have occurred at midnight on 19 April since rainfall was observed from 22:00 on 19 April to 00:00 on 20 April (Fig. 6d).

Although the simulated wind speed was overestimated during the daytime on 18 and 19 April, the simulated wind speed was very close to the observed wind during the nighttime (Fig. 6a). The overestimated wind in the afternoon of 19 April probably led to the underestimation of synchronous PM<sub>2.5</sub> (Fig. 6f). Even though the simulated and observed temperatures were close to each other (Fig. 6c), RH was underestimated from the afternoon on 19 April to the night of 20 April (Fig. 6d–e). The

underestimation of RH might be one of the reasons for the underestimation of synchronous NO<sub>3</sub><sup>-</sup> and thus PM<sub>2.5</sub> from the afternoon of 19 April to the night of 20 April (Fig. 6f).

Although the simulated maximum O<sub>3</sub> was close to observations at noon on 19 April, it was slightly overestimated around noon on 18 April and obviously overestimated on 20 April (Fig. 6g). NO was overestimated around the morning rush hour on 18 April and 20 April (Fig. 6h). The obvious overestimated O<sub>3</sub> on 20 April caused the subsequent underestimation of NO in the afternoon (Fig. 6h) and overestimation of NO<sub>2</sub> in the evening of that day (Fig. 6i).

From 18 to 20 April, the unresolved PM<sub>2.5</sub> (other in Fig. 6k, this was the unresolved species that could not be analyzed by ion chromatography or carbon analyzer, such as metals, silicate, carbonate, phosphate, etc.) was the major PM<sub>2.5</sub> species except from the night of 18 April to the morning of 19 April and around noon on 20 April, in which NO<sub>3</sub><sup>-</sup> was the major species (Fig. 6k). The trend of NO<sub>3</sub><sup>-</sup> was almost the same as that of PM<sub>2.5</sub> (Fig. 6k and f). The high O<sub>3</sub> concentration along with high HNO<sub>3</sub> and OH and low NO<sub>2</sub> concentrations revealed that the abundant HNO<sub>3</sub> was from photochemical reactions (Fig. 6l). However, the daytime NO<sub>3</sub><sup>-</sup> was not as high as expected (Fig. 6k, n), which was due to the high daytime temperature that caused NO<sub>3</sub><sup>-</sup> to tend to exist in the gas phase instead of the aerosol phase.

From night on the 18th to early morning on the 19th, the temperature was lower than that during the daytime, and NO<sub>3</sub><sup>-</sup> in the gas phase tended to condense to the aerosol phase. Therefore, HNO<sub>3</sub> was very low, and NO<sub>3</sub><sup>-</sup> was relatively high. O<sub>3</sub> formed during the daytime was titrated by NO at night and formed NO<sub>2</sub> that further reacted with O<sub>3</sub> and formed NO<sub>3</sub> radicals (Fig. 6m). NO<sub>3</sub> rapidly reacted with NO<sub>2</sub> and formed N<sub>2</sub>O<sub>5</sub> (Fig. 6m). Moreover, the heterogeneous reaction of AH<sub>2</sub>O (Fig. 6n) and N<sub>2</sub>O<sub>5</sub> formed HNO<sub>3</sub> (Fig. 6l). The RH was also high on that night, which formed higher AH<sub>2</sub>O on PM<sub>2.5</sub> (Fig. 6n). Around midnight, HNO<sub>3</sub> was low, but NO<sub>3</sub><sup>-</sup> was high, which indicates that HNO<sub>3</sub> had already reacted with NH<sub>3</sub> and formed NH<sub>4</sub>NO<sub>3</sub> on existing particles or that daytime NO<sub>3</sub><sup>-</sup> condensed to the aerosol phase. AH<sub>2</sub>O benefited the heterogeneous reactions, which could have been the major formation pathway for the formation of NO<sub>3</sub><sup>-</sup> at approximately midnight. When the AH<sub>2</sub>O concentration increased from midnight on the 18th to early morning on the 19th (Fig. 6o), NO<sub>3</sub><sup>-</sup> also increased and exceeded SO<sub>4</sub><sup>2-</sup> and “other” simultaneously (Fig. 6k). From the afternoon on the 19th to the afternoon on the 20th, the simulated RH was underestimated (Fig. 6e); thus, the AH<sub>2</sub>O was also low (Fig. 6n), which did not benefit the heterogeneous reaction.

Because the deliquescent relative humidities of NO<sub>3</sub><sup>-</sup> and SO<sub>4</sub><sup>2-</sup> were 64.6% and 80.7%, respectively, and the proportion of NO<sub>3</sub><sup>-</sup> in PM<sub>2.5</sub> was higher than that of SO<sub>4</sub><sup>2-</sup>, the mutual deliquescent relative humidity of their mixture would have been early 60% (Sun et al., 2018). Thus, in the high humidity environment (observed and simulated RHs were both higher than 80% at approximately midnight on the 18th), the PM<sub>2.5</sub> was highly hygroscopic. Abundant AH<sub>2</sub>O on the surface of particles benefited heterogeneous reactions. In addition, from night on the 18th to early morning on the 19th, HONO increased along with AH<sub>2</sub>O. It is possible that HONO was also formed through heterogeneous reactions. This kind of nocturnal HONO could be one of the sources of OH during the next day (Perner and Platt, 1979).

However, it seems that the NO<sub>3</sub><sup>-</sup> formation process was not as evident from the night of the 19th to the early morning of the 20th (Fig. 6k). The most notable characteristic is that only a very small amount of N<sub>2</sub>O<sub>5</sub> was formed at that time (Fig. 6m). The lower N<sub>2</sub>O<sub>5</sub> formation was due to fewer NO<sub>3</sub> radicals formed (Fig. 6m).

### 3.4. Sensitivity tests of different precursor emissions

In this section, we targeted 5 p.m. 2.5 events in which the PM<sub>2.5</sub> daily average concentration  $\geq 35 \mu\text{g m}^{-3}$  and the R values of hourly observed and simulated PM<sub>2.5</sub> concentrations were above 0.6: CY on 1 April, ZM and DL on April 19, and BQ and CY on 25 April (Table S6, Table S7). This

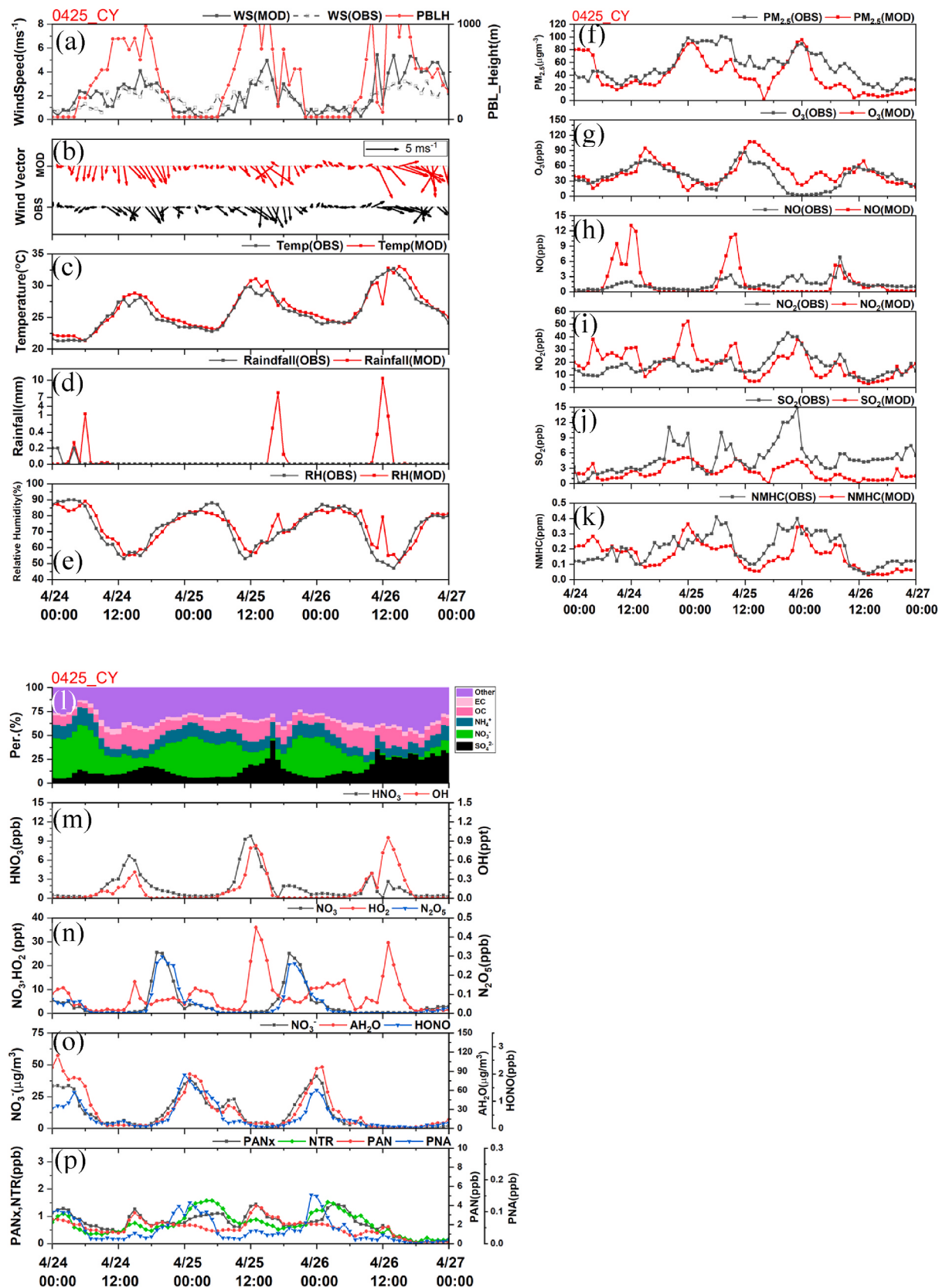


**Fig. 5.** The temporal evolution of (a) WD/WS, PBLH (b) wind vector (c) Temperature (d) Rainfall (e) Relative humidity (f) PM<sub>2.5</sub> (g) O<sub>3</sub> (h) NO (i) NO<sub>2</sub> (j) SO<sub>2</sub> (k) NMHC (l) Percentage composition of PM<sub>2.5</sub> species in total PM<sub>2.5</sub> (m) HNO<sub>3</sub>, OH (n) NO<sub>3</sub>, HO<sub>2</sub>, N<sub>2</sub>O<sub>5</sub> (o) NO<sub>3</sub><sup>-</sup>, AH<sub>2</sub>O, HONO (p) PNA, PAN, PAN<sub>x</sub>, and NTR at the CY site from 00:00 (LST) 24 April to 00:00 27 April 2017.

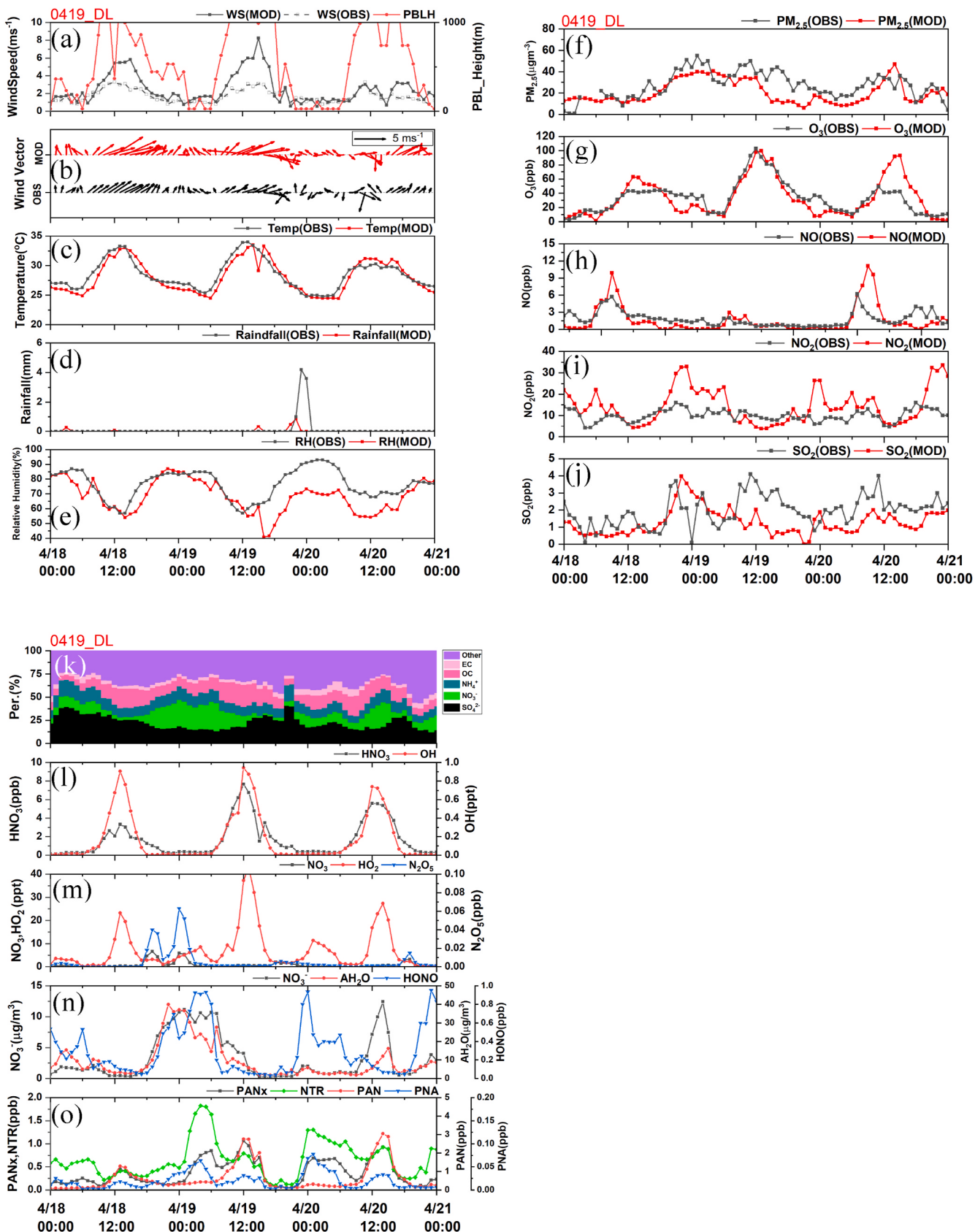


**Fig. 6.** The temporal evolution of (a) WD/WS, PBLH (b) wind vector (c) Temperature (d) Rainfall (e) Relative humidity (f)  $\text{PM}_{2.5}$  (g) O<sub>3</sub> (h) NO (i) NO<sub>2</sub> (j) SO<sub>2</sub> (k) Percentage composition of PM<sub>2.5</sub> species in total PM<sub>2.5</sub> (l) HNO<sub>3</sub>, OH (m) NO<sub>3</sub>, HO<sub>2</sub>, N<sub>2</sub>O<sub>5</sub> (n) NO<sub>3</sub><sup>-</sup>, AH<sub>2</sub>O, HONO (o) PNA, PAN, PAN<sub>X</sub>, and NTR at the DL site from 00:00 (LST) 18 April to 00:00 21 April 2017.

study conducted eight sensitivity tests and compared them with the base case. They included NMHC emissions multiplied by 2 and 0.5, denoted NMHC:200% and NMHC:50%, respectively. The other tests are denoted NO<sub>x</sub>: 200% and NO<sub>x</sub>: 50%, SO<sub>2</sub>: 200% and SO<sub>2</sub>: 50%, and NH<sub>3</sub>: 200% and NH<sub>3</sub>: 50%, in which the emissions were also multiplied by 2 and 0.5, respectively. Because the responses of NO<sub>3</sub><sup>-</sup> and other major PM<sub>2.5</sub> species formation could be influenced by each other, the following discussion is not limited to NO<sub>3</sub><sup>-</sup> but also the responses of O<sub>3</sub> and other PM<sub>2.5</sub> species, such as SO<sub>4</sub><sup>2-</sup>, OC, and NH<sub>4</sub><sup>+</sup>, to changes in precursor emissions.

As illustrated in Fig. 7a1-a5, the increase in NMHC emissions (NMHC:200%) increased the most O<sub>3</sub> around noon at most sites, probably because these sites were located in VOCs-limited regions (Chang

and Chen, 2002; urban cities in the northern Taiwan air shed, central Taiwan air shed, Kaohsiung-Pingtung air shed (in southern Taiwan), and Yulin-Chaiyi-Tainan (in southwestern Taiwan) air shed; Shiu et al., 2007: southern Taiwan; Chuang et al., 2013: Taoyuan city (in northern Taiwan); and Chang et al. (2021): northern Taiwan). For the above-mentioned 5 p.m.2.5 events, including the day before and after (Fig. 7a1-7a5), the 3-day (applicable for the following in this section) average O<sub>3</sub> concentration increased by 12.4%~26.3%. Similarly, the decrease in NO<sub>x</sub> emissions (NO<sub>x</sub>:50%) had a similar effect, which led to high O<sub>3</sub> at noon followed by NMHC:200% and increased the average O<sub>3</sub> concentration by 4.6%~23.1%. In contrast, since most sites were located in VOCs-limited regions, NO<sub>x</sub>:200% caused the least O<sub>3</sub>, followed by NMHC:50%, The average O<sub>3</sub> concentrations increased by

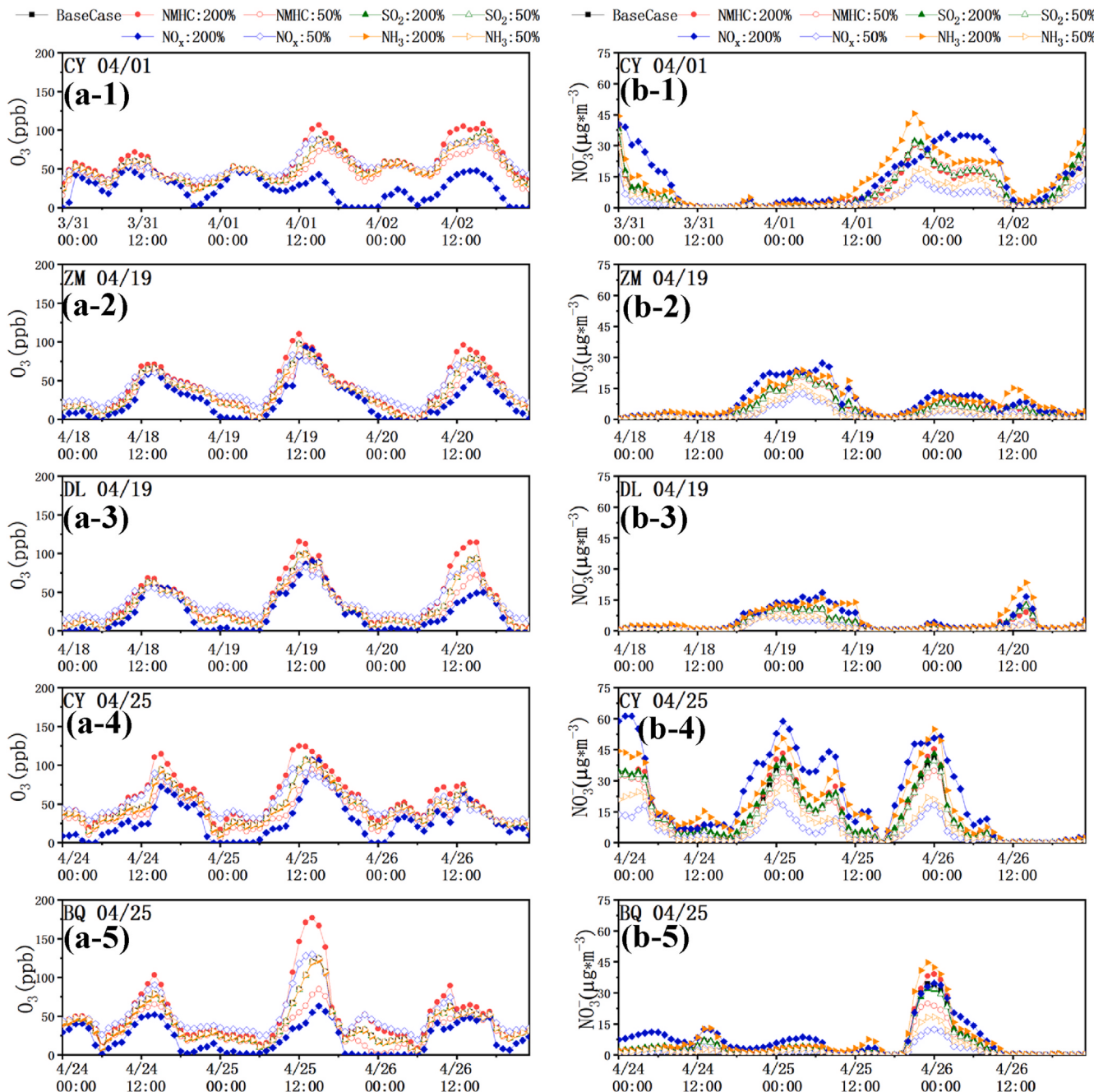


**Fig. 7.** The response of (a) O<sub>3</sub> (b) NO<sub>3</sub><sup>-</sup> at the (1) CY site on 1 April (2) ZM site on 19 April (3) DL site on 19 April (4) CY site on 19 April (5) BQ site on 25 April to the changes in NMHC, NO<sub>x</sub>, SO<sub>2</sub>, and NH<sub>3</sub> emissions, the day before and after are also included; 200% and 50% indicate that the emissions were multiplied by 2 and 0.5, respectively.

30.6%~52.5% and 10.2%~19.8%, respectively. In addition, the simulation showed that the increase/decrease in  $\text{SO}_2$  emissions led to a very small amount of less/more  $\text{O}_3$  production. Similarly, increased/decreased  $\text{NH}_3$  emissions also led to very small amounts of less/more  $\text{O}_3$ . This implies that more  $\text{O}_3$  was consumed by more  $\text{NO}_x$ ,  $\text{SO}_2$  or  $\text{NH}_3$  emissions during the formation of secondary inorganic aerosols, but more  $\text{O}_3$  was produced by more NMHC emission during the formation of secondary organic aerosols (Seinfeld and Pandis, 2006).

In Fig. 7b1-7b5, it is obvious that doubling  $\text{NO}_x$  emissions ( $\text{NO}_x:200\%$ ) or doubling  $\text{NH}_3$  emissions ( $\text{NH}_3:200\%$ ) directly caused the greatest increase in the  $\text{NO}_3^-$  concentration, especially from night to the next morning. In average,  $\text{NO}_3^-$  concentration increased by 47.6%~82.4% for the 5 p.m.<sub>2.5</sub> events. Although increased  $\text{NO}_x$  emission could reduce  $\text{O}_3$  concentration in VOC<sub>S</sub>-limited areas, it could also increase  $\text{NO}_3^-$  concentration. The increased  $\text{NH}_3$  emission could also increase  $\text{NO}_3^-$  by 41.4%~66.7%. In contrast, halving the  $\text{NO}_x$  emissions ( $\text{NO}_x:50\%$ ) led to the lowest  $\text{NO}_3^-$  concentration (decrease of 47.1%~60.8%), followed by halving the  $\text{NH}_3$  emissions ( $\text{NH}_3:50\%$ , decrease of 39.9%~45.9%). The reason for this is that  $\text{NH}_4\text{NO}_3$  is the major compound for  $\text{NO}_3^-$ , which is directly related to the major precursors  $\text{NO}_x$  and  $\text{NH}_3$ . If  $\text{NO}_x$  and  $\text{NH}_3$  emissions remained the same as in the base case, the NMHC:200% leading to the highest  $\text{O}_3$  at noon led to more production of  $\text{NO}_3^-$  than in the remaining cases. It is found that the most positive impact of NMHC:200% on  $\text{NO}_3^-$  occurred mainly when  $\text{NO}_3^-$  concentration peaked at nighttime and contributed to an increase of about 5%~15%. In contrast, the NMHC:50% produced less  $\text{NO}_3^-$  than the remaining cases. Halving  $\text{NO}_x$  emissions could have led to a reduction in  $\text{NO}_3^-$ , but it could also have led to high  $\text{O}_3$  and therefore  $\text{NO}_3^-$ , because it is not always that reducing  $\text{NO}_x$  emissions would decrease  $\text{NO}_3^-$  (Pye et al., 2009). Apparently, the effect of  $\text{NO}_x:50\%$  had a greater reduction in  $\text{NO}_3^-$  than production due to high  $\text{O}_3$ . Therefore, it is possible that there was a balancing point between the reduction and production of  $\text{NO}_3^-$  for a specific decrease in  $\text{NO}_x$  emissions. To find such a balancing point would need many scenarios of sensitivity tests to the changes in the emissions of precursors. Moreover, the balancing points could be different in various areas, which could be a complicated issue. Apparently, a comprehensive design is needed to solve this difficult issue in the future.

Doubling of NMHC emissions (NMHC:200%) increased  $\text{O}_3$  and led to the most formation of OC (Fig. S15a1-a5), which was due to the additional formation of SOA. The NMHC:200% increased OC concentration by 4.7%~12.2% in average. While halving of  $\text{NO}_x$  emissions ( $\text{NO}_x:50\%$ ) may have positive or negative impact on SOA. It is found the most increase of SOA for  $\text{NO}_x:50\%$  occurred usually from 07:00 to 13:00, the highest at noon. In contrast, the doubling of  $\text{NO}_x$  emissions ( $\text{NO}_x:200\%$ ) decreased  $\text{O}_3$  and led to the least formation of OC, followed by halving of NMHC emissions (NMHC:50%). The  $\text{NO}_x:200\%$  decreased OC concentration by 10.9%~19.6% in average, usually the highest at noon as well. On average, the formation of  $\text{NO}_3^-$  (Fig. 7b1-7b5) was higher than that of OC for the NMHC and  $\text{NO}_x$  emission change tests during the PM<sub>2.5</sub> event (Fig. S15a1-a5). The change in  $\text{SO}_2$  emissions ( $\text{SO}_2:200\%$  and  $\text{SO}_2:50\%$ ) and change in  $\text{NH}_3$  emissions ( $\text{NH}_3:200\%$  and  $\text{NH}_3:50\%$ ) had very small effects on the formation of OC.

An increase or decrease in  $\text{SO}_2$  emissions would have directly led to an increase or decrease in  $\text{SO}_4^{2-}$  formation. The average increase of  $\text{SO}_4^{2-}$  concentration was 32.3%~54.6%. In addition, theoretically, an increase in  $\text{NO}_x$  emissions ( $\text{NO}_x:200\%$ ) would have produced abundant  $\text{HNO}_3$ , which competes for  $\text{NH}_3$  with  $\text{H}_2\text{SO}_4$  and hinders the formation of ammonium sulfate; a decrease in  $\text{NO}_x$  emissions ( $\text{NO}_x:50\%$ ) would have produced less  $\text{HNO}_3$  and would have benefited the formation of ammonium sulfate. From Fig. S15b1-b5, it is not absolute, but for most times, doubling  $\text{NO}_x$  emissions led to less  $\text{SO}_4^{2-}$ . Similarly, more/less  $\text{NH}_3$  emissions led to more/less  $\text{SO}_4^{2-}$ , but relatively more/less NMHC had less effect on  $\text{SO}_4^{2-}$  formation.

The increase or decrease in  $\text{NH}_3$  emissions was not absolutely related to the highest or lowest formation of  $\text{NH}_4^+$ , as illustrated in Fig. S15c1-

c5. The  $\text{NH}_3:200\%$  and  $\text{NH}_3:50\%$  increased and decreased  $\text{NH}_4^+$  by 22.0%~36.2% and 22.2%~29.3% in average, respectively. Instead,  $\text{NH}_4^+$  formation was also positively correlated with  $\text{NO}_x$  and  $\text{SO}_2$  emissions, which explains the corresponding production/reduction of  $\text{NH}_4\text{NO}_3$  and ammonium sulfate. The  $\text{SO}_2:200\%$  and  $\text{SO}_2:50\%$  increased and decreased  $\text{NH}_4^+$  by 21.9%~26.5% and 12.0%~18.9% in average, respectively;  $\text{NO}_x:200\%$  and  $\text{NO}_x:50\%$  increased and decreased  $\text{NH}_4^+$  by 16.6%~57.8% and 15.4%~39.8% in average, respectively. In contrast, the modification of NMHC emissions had less influence on the formation of  $\text{NH}_4^+$ .

### 3.5. Pathways attributed to $\text{HNO}_3$ formation during PM<sub>2.5</sub> events

Again, the discussion of  $\text{HNO}_3$  formation pathways is limited to those 5 p.m.<sub>2.5</sub> events: CY on 1 April, ZM and DL on April 19, and BQ and CY on 25 April in this section. The formulas listed in Section 2.4 are the  $\text{HNO}_3$  formation pathways considered in the simulation.

From Fig. 8a-e, it is obvious that the oxidation reaction of OH and  $\text{NO}_2$  (R1,  $\text{HNO}_3\text{OHNO}_2$ ) accounted for more than 90% of  $\text{HNO}_3$  formation during the daytime, and the proportion of the oxidation reaction contribution during the daytime was approximately the same at different sites/latitudes. However, the attribution of the oxidation reaction to  $\text{HNO}_3$  formation during the nighttime was more or less at different sites/latitudes during different PM<sub>2.5</sub> events. Since  $\text{HO}_2$  was mainly produced during the daytime (Figs. 5n and 6m), the gain of  $\text{HNO}_3$  from the reaction of NO and  $\text{HO}_2$  radicals (R6,  $\text{HNO}_3\text{NOHO}_2$ ) was approximately 3% during the daytime and less than 1% at night.

From evening to the next early morning, the heterogeneous reaction of  $\text{N}_2\text{O}_5$  (R2,  $\text{HET-N}_2\text{O}_5$ ) was the main contributor to  $\text{HNO}_3$  formation, from 30% to more than 90%, as illustrated in Fig. 8a-e. The contribution was the highest at CY exceeding 90% of the total  $\text{HNO}_3$  during the nighttime, which was probably because CY was located in a lower latitude area than the DL, ZM, and BQ sites. The homogeneous reaction of  $\text{N}_2\text{O}_5$  (R3,  $\text{HNO}_3\text{N}_2\text{O}_5$ ) also mainly occurred at night due to high relative humidity and probably contributed from nearly zero to 11% of the total  $\text{HNO}_3$  production. The reaction of hydrocarbons and  $\text{NO}_3$  radicals (R4,  $\text{HET-HCNO}_3$ ) also contributed more  $\text{HNO}_3$  at night than during the day because  $\text{NO}_3$  was produced more and  $\text{AH}_2\text{O}$  was higher at night than during the day.

The gain of  $\text{HNO}_3$  from the reduction reaction of organic nitrate (R5,  $\text{HNO}_3\text{NO}_3\text{HC}$ ) reached nearly zero to 14% at night, which was higher than that produced during the daytime, which was less than 3% of the total  $\text{HNO}_3$  production because  $\text{NO}_3$  was produced more at night than during the day. Although the reaction of  $\text{NO}_3$  and  $\text{HO}_2$  radicals (R7,  $\text{HNO}_3\text{NO}_3\text{HO}_2$ ) produced more  $\text{HNO}_3$  at night, the contribution to  $\text{HNO}_3$  was less than 1%, which can almost be ignored compared with other formation pathways. The reaction of  $\text{NO}_3$  and  $\text{HO}_2$  radicals (R7,  $\text{HNO}_3\text{NO}_3\text{HO}_2$ ) also produced more  $\text{HNO}_3$  at night, and the contribution to  $\text{HNO}_3$  was usually less than 1%, which can almost be ignored.

From Fig. 8f-j, it is obvious that gas-phase  $\text{HNO}_3$  was more than or comparable to aerosol-phase  $\text{NO}_3^-$  ( $\text{ANO}_3$  in Fig. 8f-j) during the daytime. When the temperature decreased from noon to night,  $\text{HNO}_3$  gradually decreased; in contrast,  $\text{ANO}_3$  was produced considerably during the nighttime. The  $\text{ANO}_3$  concentration during the nighttime was much higher than or equal to the total  $\text{NO}_3^-$  ( $\text{ANO}_3+\text{HNO}_3$ ) during the daytime. This explains why heterogeneous reactions during nighttime were the main cause of high  $\text{NO}_3^-$  (or PM<sub>2.5</sub>) concentrations in these PM<sub>2.5</sub> events.

### 3.6. The relationship of daytime and nighttime simulated $\text{HNO}_3$ and its precursors

From the analysis in Sections 3.3 to 3.5, we can conclude that the oxidation reaction of  $\text{NO}_2$  and OH during the daytime and the heterogeneous reaction of  $\text{N}_2\text{O}_5$  during the nighttime were the major contributions to  $\text{HNO}_3$ . Thus, this study attempts to test the correlations

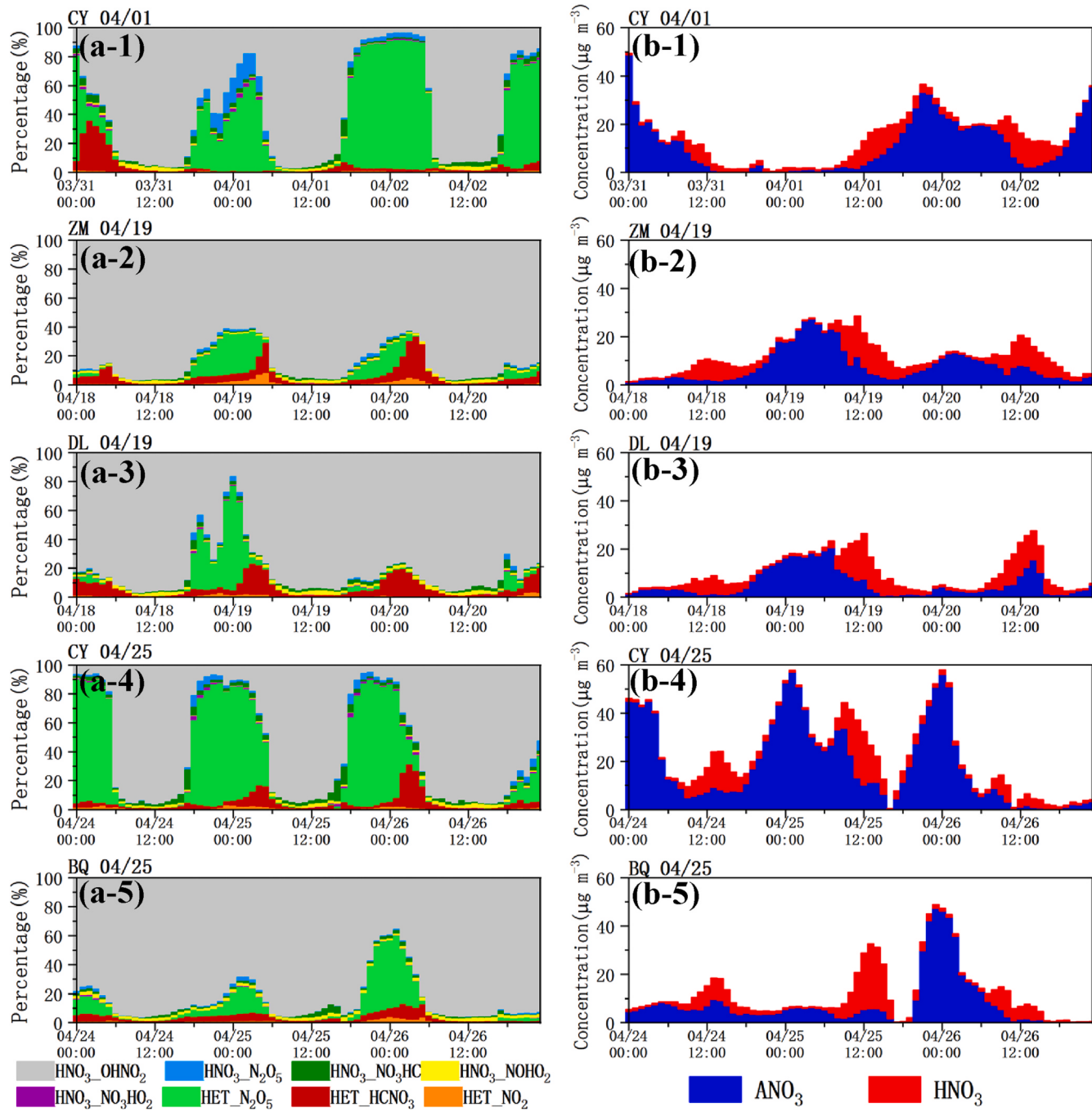


**Fig. 8.** Attribution to (a) HNO<sub>3</sub> formation pathways and (b) aerosol phase (ANO<sub>3</sub>)/gas phase (HNO<sub>3</sub>) nitrate at (1) CY site on 1 April (2) ZM site on 19 April (3) DL site on 19 April (4) CY site on 19 April (5) BQ site on 25 April, the day before and after are also included.

between precursors and intermediate products that participate in the formation of the final product, HNO<sub>3</sub>, via these two pathways. We selected the simulated maximum values of the species participating in these two pathways from two periods: daytime (06:00–18:00) and nighttime (18:00–06:00). Then, we determined the linear relationships between them for daytime and nighttime periods individually. Because O<sub>3</sub> was low during the nighttime, the daytime maximum O<sub>3</sub> was also used in the correlation analysis for the nighttime period. The statistical significance of the linear regressions is listed in Table S8.

For the daytime oxidation reactions, it was found that the R value between O<sub>3</sub> and HNO<sub>3</sub> (Fig. 9a2-e2) was between 0.71 and 0.94, obviously higher than the other combinations including O<sub>3</sub>-OH (0.04–0.42, Fig. 9a1-e1), OH-HNO<sub>3</sub> (-0.06–0.45, Fig. 9a3-e3), and NO<sub>2</sub>-HNO<sub>3</sub>

(0.03–0.44, Fig. 9a4-e4). This explains the higher O<sub>3</sub> reached around the noon period, and the higher HNO<sub>3</sub> formed almost at the same time. In contrast, the daytime maximum NO<sub>2</sub> concentration around the morning rush hour was not highly correlated with daytime-formed HNO<sub>3</sub>.

For the nighttime heterogeneous reaction, the highest R value exists between NO<sub>3</sub> and N<sub>2</sub>O<sub>5</sub>, from 0.73 to 0.96 (Fig. 10a3-e3), followed by NO<sub>3</sub> and HNO<sub>3</sub> from 0.31 to 0.82 (Fig. 10a6-e6), N<sub>2</sub>O<sub>5</sub> and HNO<sub>3</sub> from 0.40 to 0.81 (Fig. 10a7-e7), then O<sub>3</sub> and NO<sub>3</sub>, from 0.49 to 0.70 (Fig. 10a1-e1), O<sub>3</sub> and N<sub>2</sub>O<sub>5</sub> from 0.47 to 0.75 (Fig. 10a2-e2), and O<sub>3</sub> and HNO<sub>3</sub> from 0.34 to 0.68 (Fig. 10a5-e5). From the above, we can see that the daytime maximum O<sub>3</sub> was moderately to highly correlated with the nighttime species on the pathway of heterogeneous reactions. This implies that daytime-formed O<sub>3</sub> participating in the formation of

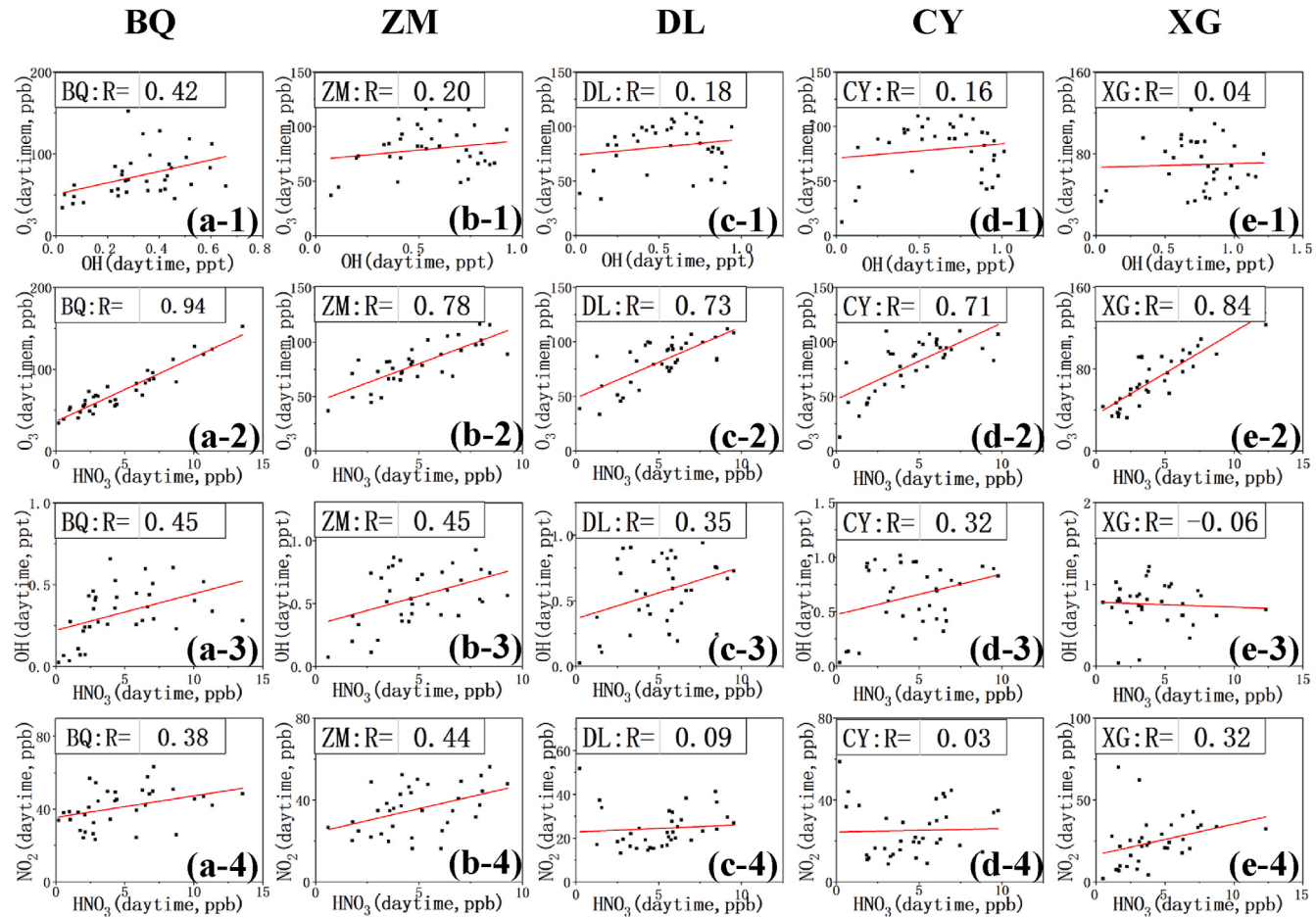


**Fig. 9.** The scatter plots of daytime (06:00–18:00) maximum HNO<sub>3</sub> and its main precursors and intermedia products at (a) BQ (b) ZM (c) DL (d) CY (e) XG sites for (1) O<sub>3</sub>-OH (2) O<sub>3</sub>-HNO<sub>3</sub> (3) OH-HNO<sub>3</sub> (4) NO<sub>2</sub>-HNO<sub>3</sub>. All species are daytime maximum concentrations.

nighttime HNO<sub>3</sub> was significant. In contrast, the correlations between NO<sub>2</sub> and N<sub>2</sub>O<sub>5</sub> (0.26–0.68, Fig. 10a4–e4) and between NO<sub>2</sub> and HNO<sub>3</sub> (0.27–0.54, Fig. 10a9–e9) were low. The maximum NO<sub>2</sub> concentration around the evening rush hour or midnight was not highly correlated with nighttime maximum concentrations of intermediate products or HNO<sub>3</sub>. For the selected PM<sub>2.5</sub> events, the simulation indicated that daytime maximum O<sub>3</sub> was significantly related to daytime HNO<sub>3</sub> and nighttime HNO<sub>3</sub> instead of NO<sub>2</sub>. This implies that O<sub>3</sub> could have played a more important role in HNO<sub>3</sub> formation.

#### 4. Conclusions

From the long-term trend of NO<sub>3</sub><sup>-</sup> concentration and the proportion of NO<sub>3</sub><sup>-</sup> in PM<sub>2.5</sub>, we have realized the increasing importance of NO<sub>3</sub><sup>-</sup> in recent years. The present study applied air-quality modeling to analyze the NO<sub>3</sub><sup>-</sup> formation mechanisms and attempted to suggest the control direction. We addressed the temporal evolution of meteorological conditions, NO<sub>3</sub><sup>-</sup> formation and its precursors and intermediate products. Then, we estimated the contribution of NO<sub>3</sub><sup>-</sup> formation pathways, conducted a sensitivity test to determine the response of O<sub>3</sub> and major PM<sub>2.5</sub> species to changes in precursor emissions, and analyzed the correlation of HNO<sub>3</sub> and its precursors and intermediate products participating in the major daytime and nighttime NO<sub>3</sub><sup>-</sup> formation pathways.

This study conducted a retrospective simulation, in which 5 p.m. 2.5 events in which the daily average concentrations were  $\geq 35 \mu\text{g m}^{-3}$  and their corresponding R values of simulated and observed PM<sub>2.5</sub> were above 0.6. Two of the PM<sub>2.5</sub> events were selected to discuss the temporal evolution of the NO<sub>3</sub><sup>-</sup> formation process. In the simulation, low wind

speed and low PBLH were deterministic for the accumulation of PM<sub>2.5</sub> at night. At approximately noon, the trends of OH and HNO<sub>3</sub> were almost the same because the oxidation reaction of OH and NO<sub>2</sub> (R1) was the main NO<sub>3</sub><sup>-</sup> formation mechanism during the daytime. During the midnight period, N<sub>2</sub>O<sub>5</sub>, AH<sub>2</sub>O, NO<sub>3</sub><sup>-</sup>, and HONO synchronously peaked, which indicates that the heterogeneous reaction of N<sub>2</sub>O<sub>5</sub> (R2) was obviously the main formation mechanism of NO<sub>3</sub><sup>-</sup>. For the aforementioned 5 p.m. 2.5 events, we conducted a sensitivity test to determine their impact on different NMHC, NO<sub>x</sub>, SO<sub>2</sub>, and NH<sub>3</sub> emissions on the formation of O<sub>3</sub> and major PM<sub>2.5</sub> species. Doubling (200%) and halving (50%) the NO<sub>x</sub> and NH<sub>3</sub> emissions could directly lead to the highest and lowest production of NO<sub>3</sub><sup>-</sup>, followed by the NMHC, which influenced the production of O<sub>3</sub> the most. This suggests that in addition to the direct change in precursor emissions, O<sub>3</sub> was also an important factor for NO<sub>3</sub><sup>-</sup> formation during these PM<sub>2.5</sub> events.

Among the eight HNO<sub>3</sub> formation pathways, during the daytime, the reaction of NO<sub>2</sub> and OH (R1) accounted for more than 90% of the total HNO<sub>3</sub> at that moment. From nighttime to the early morning, the heterogeneous reaction of N<sub>2</sub>O<sub>5</sub> (R2) could account for approximately 30%–90% of the total HNO<sub>3</sub>, followed by the reduction reaction of organic nitrate (R5) from nearly zero to 14% of the contribution to HNO<sub>3</sub> and the homogeneous reaction of N<sub>2</sub>O<sub>5</sub> (R3a, R3b) from approximately zero to 11%. The next reaction was that of HCs and NO<sub>3</sub> radicals (R4), followed by the heterogeneous reaction of NO<sub>2</sub> on the surface of aerosols (R8) and reaction of NO and HO<sub>2</sub> radicals (R6), which each accounted for less than 3% of the formed HNO<sub>3</sub>. The reaction of NO<sub>3</sub> and HO<sub>2</sub> (R7) only contributed less than 1% of the formed HNO<sub>3</sub>.

For the major formation pathways during daytime, i.e., oxidation

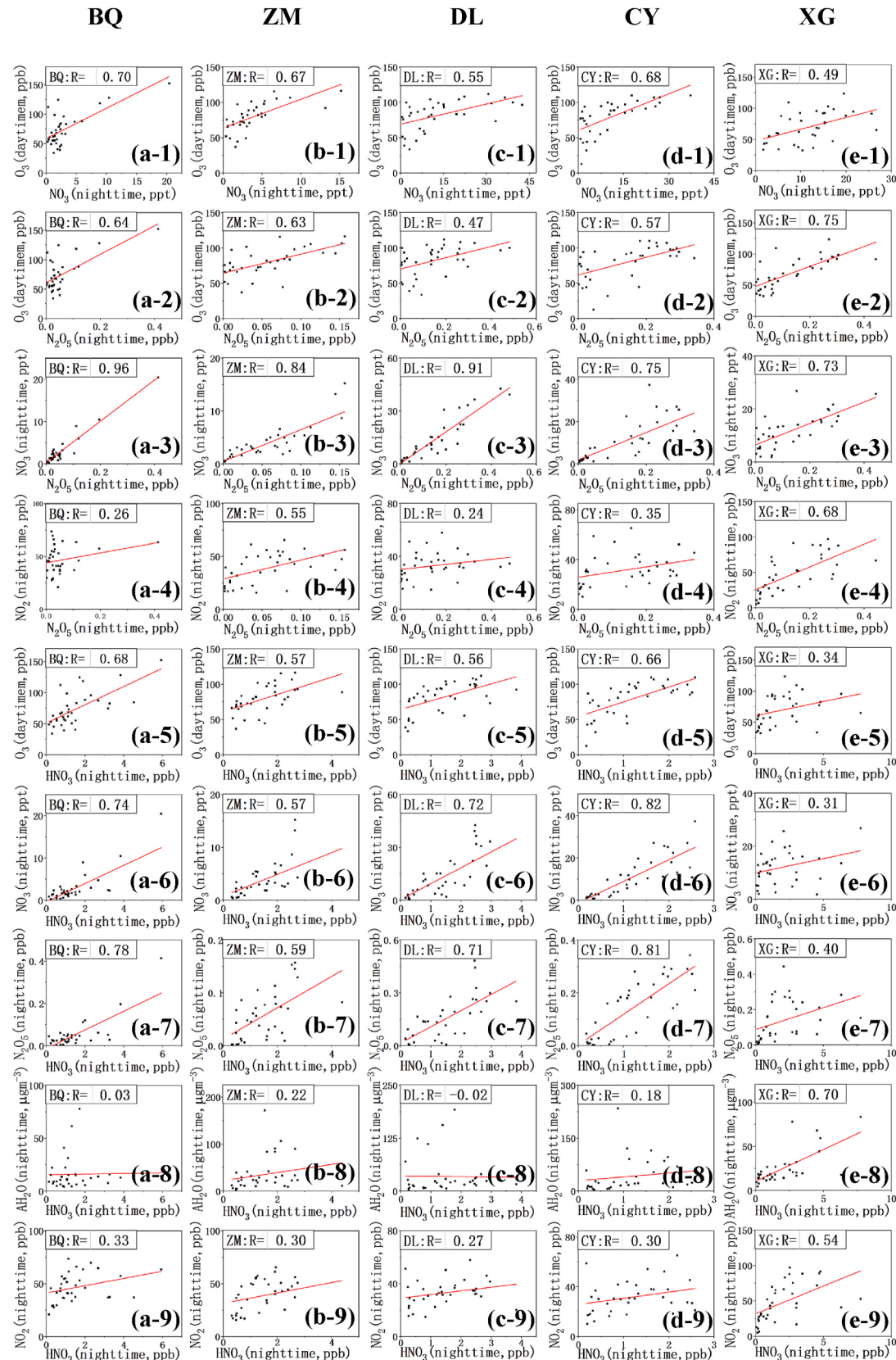


**Fig. 10.** The scatter plots of nighttime (18:00–06:00) maximum HNO<sub>3</sub> and its main precursors and intermedia products at (a) BQ (b) ZM (c) DL (d) CY (e) XG sites for (1) O<sub>3</sub>-NO<sub>3</sub> (2) O<sub>3</sub>-N<sub>2</sub>O<sub>5</sub> (3) NO<sub>3</sub>-N<sub>2</sub>O<sub>5</sub> (4) NO<sub>2</sub>-N<sub>2</sub>O<sub>5</sub> (5) O<sub>3</sub>-HNO<sub>3</sub> (6) NO<sub>3</sub>-HNO<sub>3</sub> (7) N<sub>2</sub>O<sub>5</sub>-HNO<sub>3</sub> (8) AH<sub>2</sub>O-HNO<sub>3</sub> (9) NO<sub>2</sub>-HNO<sub>3</sub>. All species are nighttime maximum concentrations except O<sub>3</sub> is daytime maximum concentration.

reactions, the R value between daytime maximum O<sub>3</sub> and daytime maximum HNO<sub>3</sub> was between 0.71 and 0.94, obviously higher than that for O<sub>3</sub>-OH, OH-HNO<sub>3</sub>, and NO<sub>2</sub>-HNO<sub>3</sub>. For nighttime heterogeneous reactions, it was found that the relationships between daytime maximum O<sub>3</sub> and nighttime maximum NO<sub>3</sub>, N<sub>2</sub>O<sub>5</sub>, and HNO<sub>3</sub> were moderately to highly correlated. Instead, NO<sub>2</sub> was poorly to moderately correlated with those intermediate products and HNO<sub>3</sub>. This implies that regardless of the daytime or nighttime, O<sub>3</sub> always played an important role in HNO<sub>3</sub> formation and could be even more important than the precursor NO<sub>2</sub>.

The sensitivity test shows that if NO<sub>x</sub> reduction is strengthened, NO<sub>3</sub><sup>-</sup> would decrease accordingly, thus reducing PM<sub>2.5</sub> in Taiwan. However, the long-term observation reveals the NO<sub>x</sub> concentrations/emission reduction in the last decade did not reduce NO<sub>3</sub><sup>-</sup>. The present simulation results have demonstrated O<sub>3</sub> plays an important role in the NO<sub>3</sub><sup>-</sup> formation, which may echo the results of Thunis et al. (2021) that the reduction in NO<sub>x</sub> emissions could increase O<sub>3</sub> in some NO<sub>x</sub>-rich areas and lead to a transitional increase in PM<sub>2.5</sub> in winter in Europe. Therefore, we suggest to re-examine the NO<sub>x</sub>-limited and VOC-limited areas because NO<sub>x</sub> reduction could directly reduce NO<sub>3</sub><sup>-</sup> or possibly increase the O<sub>3</sub> concentration in VOC-limited regions and then lead to NO<sub>3</sub><sup>-</sup> formation. How to reduce NO<sub>x</sub> emissions and reduce O<sub>3</sub> concentrations at the same time is a challenge because these two strategies could conflict if the NO<sub>x</sub> emission reduction is not correct in amount or in location. Therefore, further in-depth studies are needed for this difficult issue.

#### Credit author statement

Ming-Tung Chuang designed the experiment, carried out most parts of the study, and wrote the original draft.

Chang-Fu Wu provided beneficial consultations according to his previous publications.

Chuan-Yao Lin helped with the simulation skill and explanation of the simulation results.

Wei-Che Lin helped with the data processing and figure drawing.

Charles C.K. Chou provided PM<sub>2.5</sub> composition data from 2003 to 2009 and provided financial support.

Chung-Te Lee provided the PM<sub>2.5</sub> composition data from 2015 to 2019 and provided financial support.

Tang-Huang Lin provided opinions regarding the simulation analysis.

Joshua S. Fu provided advanced experience in CMAQ modeling analysis.

Steven Soon-Kai Kong helped draw several figures.

#### Declaration of competing interest

The authors declare that they have no known competing financial interests or personal relationships that could have appeared to influence the work reported in this paper.

#### Acknowledgments

We express deep gratitude for the support from the Ministry of Science and Technology (MOST), Academia Sinica (AS-GC-110-01) and TWEPA. The researchers acknowledge contributions from the U.S. National Center for Environmental Prediction (NCEP) and the Data Bank for Atmospheric and Hydrologic Research (managed by the Department of Atmospheric Science of Chinese Cultural University and sponsored by MOST) for input data used in the meteorological modeling and for monitoring data in the evaluation of meteorological modeling. We are also grateful to the TWEPA for their air-quality data in the evaluation of air-quality modeling.

#### Appendix A. Supplementary data

Supplementary data to this article can be found online at <https://doi.org/10.1016/j.atmosenv.2021.118856>.

#### References

- Baasandorj, M., Hoch, S.W., Bares, R., Lin, J.C., Brown, S.S., Millet, D.B., Martin, R., Kelly, K., Zarzana, K.J., Whiteman, C.D., Duke, W.P., Tonnesen, G., Jaramillo, I.C., Sohl, J., 2017. Environ. Sci. Technol. 51, 5941–5950.
- Bey, I., Jacob, D.J., Yantosca, R.M., Logan, J.A., Field, B., Fiore, A.M., Li, Q., Liu, H., Mickley, L.J., Schultz, M., 2001. Global modeling of tropospheric chemistry with assimilated meteorology: model description and evaluation. J. Geophys. Res. 106 (23), 073-23,096.
- Byun, D., Schere, K.L., 2006. Review of the governing equations, computational algorithms, and other species of the models-3 Community Multiscale Air Quality (CMAQ) modeling system. Appl. Mech. Rev. 59, 51–77.
- Chang, C.M., Chang, L.N., Hsiao, H.C., Lu, F.C., Shieh, P.F., Chen, C.N., Lu, S.C., 2006. A further study of high air pollution episodes in Taiwan using the Microwave Temperature Profiler (MTP-5HE). JSME Int. J. Ser. B 40, 60–64.
- Chang, K.H., Chen, C.H., 2002. Analysis of ozone pollution control species in Taiwan. In: 6th Air Pollution Control Conference, September 9-13, Taipei, Taiwan.
- Chang, K.H., Chen, D.F., Tsai, C.Y., 2021. Challenges of ozone (O<sub>3</sub>) pollution improvement and the upgrade with air quality. Engineering 94 (2), 59–76 in Chinese.
- Chen, C.H., Chang, K.H., Chen, T.F., 2014. Impact of long transport on Taiwan's ozone air quality from East Asia. Appl. Mech. Mater. 692, 13–21.
- Cheng, Y.F., Zheng, G.J., Wei, C., Mu, Q., Zheng, B., Wang, Z.B., Gao, M., Zhang, Q., He, K.B., Carmichael, G., Posch, U., Su, H., 2016. Reactive nitrogen chemistry in aerosol water as a source of sulfate during haze events in China. Sci. Adv. 2 (12) <https://doi.org/10.1126/sciadv.1601530>.
- Chou, C.C.K., Lee, C.T., Yuan, C.T., Hsu, W.C., Lin, C.Y., Hsu, S.C., Liu, S.C., 2008. Implications of the chemical transformation of Asian outflow aerosols for the long-range transport of inorganic nitrogen species. Atmos. Environ. 42, 7508–7519.
- Chou, C.C.K., Lee, C.T., Cheng, M.T., Yuan, C.S., Wu, Y.L., Hsu, W.C., Lung, S.C., Hsu, S.C., Lin, C.Y., Liu, S.C., 2010. Seasonal variation and spatial distribution of carbonaceous aerosols in Taiwan. Atmos. Chem. Phys. 10, 9563–9578.
- Chow, J.C., Watson, J.G., Crow, D., Lowenthal, D.H., Merrifield, T., 2001. Comparison of IMPROVE and NIOSH carbon measurements. Aerosol Sci. Technol. 34, 23–34.
- Chuang, M.T., Wang, J.L., Kuo, C.Y., Chang, S.Y., Chang, C.C., Lai, H.C., 2013. The Study of PM<sub>2.5</sub> and O<sub>3</sub> Events and Control Strategy Development. Taoyuan Environmental Protection Bureau, p. 535pp in Chinese.
- Chuang, M.T., Chiang, P.C., Chan, C.C., Wang, C.F., Chang, E.E., Lee, C.T., 2008. The effects of synoptical weather pattern and complex terrain on the formation of aerosol events in the Greater Taipei area. Sci. Total Environ. 399, 128–146.
- Chuang, M.T., Chou, C.C.K., Lin, N.H., Takami, A., Hsiao, T.C., Lin, T.H., Fu, J.S., Pani, S.K., Lu, Y.R., Yang, T.Y., 2017. A simulation study on PM<sub>2.5</sub> sources and meteorological characteristics at the northern tip of Taiwan in the early stage of the Asian haze period. Aerosol. Air. Qual. Res. 17, 3166–3178.
- Emery, C., Tai, E., Yarwood, G., 2001. Enhanced Meteorological Modeling and Performance Evaluation for Two Texas Ozone Episodes. Report to the Texas Natural Resources Conservation Commission. prepared by ENVIRON International Corp., Novato, CA.
- Emery, C., Liu, Z., Russell, A.G., Odman, M.T., Yarwood, G., Kumar, N., 2017. Recommendations on statistics and benchmarks to assess photochemical model performance. J. Air Waste Manag. Assoc. 67 (5), 582–598.
- Ge, X.L., He, Y.A., Sun, Y.L., Xu, J.Z., Wang, J.F., Shen, Y.F., Chen, M.D., 2017. Characteristics and formation mechanisms of fine particulate nitrate in typical urban areas in China. Atmosphere 8, 62. <https://doi.org/10.3390/atmos8030062>.
- Grell, G.A., Peckham, S.E., Schmitz, R., McKeen, S.A., Frost, G., Skamarock, W.C., Eder, B., 2005. Fully coupled "online" chemistry within the WRF model. Atmos. Environ. 39, 6957–6975.
- Guenther, A.B., Jiang, X., Heald, C.L., Sakulyanontvittaya, T., Duhl, T., Emmons, L.K., Wang, X., 2012. The Model of Emissions of Gases and Aerosols from Nature version 2.1 (MEGAN2.1): an extended and updated framework for modeling biogenic emissions. Geosci. Model Dev. (GMD) 5, 1471–1492.
- Ho, Y.C., 2015. Effects of Environment Area on the Mixing Height and Ozone Concentrations Distribution in Taiwan. Master thesis, Department of Environmental Engineering and Science, Fooyin University in Chinese.
- Houyoux, M.R., Vukovich, J.M., 1999. Updates to the sparse Matrix operator Kernel emissions (smoke) modeling system and integration with models-3. In: Emissions Inventory: Regional Strategies for the Future Conference. Air & Waste Management Association, Raleigh, North Carolina.
- Huang, L., Zhu, Y., Zhai, H., Xue, S., Zhu, T., Shao, Y., Liu, Z., Emery, C., Yarwood, G., Wang, Y., Fu, J., Zhang, K., Li, L., 2021. Recommendations on benchmarks for numerical air quality model applications in China – Part 1: PM<sub>2.5</sub> and chemical species. Atmos. Chem. Phys. 21, 2725–2743.
- Kelley, J.T., Jang, C., Zhu, Y., Long, S., Xing, J., Wang, S., Murphy, B.N., Pye, H.O.T., 2021. Predicting the nonlinear response of PM<sub>2.5</sub> and O<sub>3</sub> to precursor emission changes with a response surface model. Atmosphere 12, 1044.
- Kim, Y.J., Spak, S.N., Carmichael, G.R., Riemer, N., Stanier, C.O., 2014. Modeled aerosol nitrate formation pathways during wintertime in the Great Lakes region of North America. J. Geophys. Res. 119, 12420–12445.

- Kuprov, R.; Eatough, D. J.; Cruickshank, T.; Olson, N.; Cropper, P. M.; Hansen, J. C. Composition and secondary formation of fine particulate matter in the Salt Lake Valley: winter 2009. *J. Air Waste Manag. Assoc.* 64 (8), 957–969.
- Lee, C.T., Chou, C.C.K., Chang, S.Y., Hsiao, T.C., Chuang, M.T., Hsu, W.C., 2020. The 2020 Project of Chemical Speciation Monitoring and Analysis of Fine Particulate Matter (PM2.5), p. 414pp.
- Li, M., Zhang, Q., Kurokawa, J., Woo, J.H., He, K.B., Lu, Z.F., Ohara, T., Song, Y., Streets, D.G., Carmichael, G.R., Cheng, Y.F., Hong, C.P., Huo, H., Jiang, X.J., Kang, S.C., Liu, F., Su, H., Zheng, B., 2017. MIX: a mosaic Asian anthropogenic emission inventory under the international collaboration framework of the MICS-Asia and HTAP. *Atmos. Chem. Phys.* 17, 935–963.
- Loftus, C., Yost, M., Sampson, P., Arias, G., Torres, E., Vasquez, V.B., Bhatti, P., Karr, C., 2015. Regional PM2.5 and asthma morbidity in an agricultural community: a panel study. *Environ. Res.* 136, 505–512.
- Pani, S.K., Wang, S.H., Lin, N.H., Tsay, S.C., Lolli, S., Chuang, M.T., Lee, C.T., Chantara, S., Yu, J.Y., 2016. Assessment of aerosol optical property and radiative effect for the layer decoupling cases over the northern South China Sea during the 7-SEAS/Dongsha Experiment. *J. Geophys. Res.* 121, 4894–4906.
- Perner, D., Platt, U., 1979. Detection of nitrous-acid in the atmosphere by differential optical-absorption. *Geophys. Res. Lett.* 6, 917–920.
- Pye, H.O., Liao, T., Wu, H.S., Mickley, L.J., Jacob, D.J., Henze, D.K., Seinfeld, J.H., 2009. Effect of changes in climate and emissions on future sulfate-nitrate-ammonium aerosol levels in the United States. *J. Geophys. Res.* 114, D01205. <https://doi.org/10.1029/2008JD010701>.
- Qu, Y., Chen, Y., Liu, X., Zhang, J., Guo, Y., An, J., 2019. Seasonal effects of additional HONO sources and the heterogeneous reactions of N<sub>2</sub>O<sub>5</sub> on nitrate in the North China Plain. *Sci. Total Environ.* 690, 97–107.
- Seinfeld, J.H., Pandis, S.N., 2006. *Atmospheric Chemistry and Physics: from Air Pollution to Climate Change*. John Wiley & Sons, New York, NY, USA.
- Shiu, C.J., Liu, S.C., Chang, C.C., Chen, J.P., Chou, C.C.K., Lin, C.Y., Young, C.Y., 2007. Photochemical production of ozone and control strategy for Southern Taiwan. *Atmos. Environ.* 41, 9324–9340.
- Simpson, D., Benedictow, A., Berge, H., Bergström, R., Emberson, L.D., Fagerli, H., Flechard, C.R., Hayman, G.D., Gauss, M., Jonson, J.E., Jenkin, M.E., Nyri, A., Richter, C., Semeena, V.S., Tsyro, S., Tuovinen, J.P., Valdebenito, Á., Wind, P., 2012. The EMEP MSC-W chemical transport model – technical description. *Atmos. Chem. Phys.* 12, 7825–7865.
- Skamarock, C., Klemp, B., Dudhia, J., Gill, O., Barker, D.E., Ekda, G., Huang, X.-Y., Wang, W., Powers, G., 2008. A Description of the Advanced Research WRF Version 3. National Center for Atmospheric Research, Boulder, p. 125pp.
- Song, Y.Y., Chen, G.X., Wang, W.C., 2019. Aerosol direct radiative and cloud adjustment effects on surface climate over eastern China: analyses of WRF model simulations. *J. Clim.* 32, 1293–1306.
- Sun, J.X., Liu, L., Xu, L., Wang, Y.Y., Wu, Z.J., Hu, M., Shi, Z.B., Li, Y.J., Zhang, X.Y., Chen, J.M., Li, W.J., 2018. Key role of nitrate in phase transitions of urban particles: implications of important reactive surfaces for secondary aerosol formation. *J. Geophys. Res.* 123, 1234–1243.
- TWEPA, 2016. New air quality modeling and simulation standards. Effective on 1st January 2016. <https://oaout.epa.gov.tw/Law/LawContent.aspx?id=GL005316>.
- TWEPA, 2017. Building of the taiwan emission data system. Taiwan EPA report. <https://teds.epa.gov.tw/>.
- Thunis, P., Clappier, A., Beekmann, M., Putaud, J.P., Cuvelier, C., Madrazo, J., de Meij, A., 2021. Non-linear response of PM2.5 to changes in NOX and NH3 emissions in the Po basin (Italy): consequences for air quality plans. *Atmos. Chem. Phys.* 21, 9309–9327.
- Vukovich, J., Pierce, T., 2002. The implementation of BEIS3 within the SMOKE modeling framework. In: Proceedings of the 11th International Emissions Inventory Conference, Atlanta, Georgia.
- Wang, H.J., Chen, H.P., 2016. Understanding the recent trend of haze pollution in eastern China: roles of climate change. *Atmos. Chem. Phys.* 16, 4205–4211.
- Yao, T., Fung, J.C.H., Ma, H., Lau, A.K.H., Chan, P.W., Yu, J.Z., Xue, J., 2014. Enhancement in secondary particulate matter production due to mountain trapping. *Atmos. Res.* 147, 227–236.
- Zhai, S., Jacob, D.J., Wang, X., Liu, Z., Wen, T., Shah, V., Li, K., Moch, J.M., Bates, K.H., Song, S., Shen, L., Zhang, Y., Luo, G., Yu, F., Sun, Y., Wang, L., Qi, M., Tao, J., Gui, K., Xu, H., Zhang, Q., Zhao, T., Wang, Y., Lee, H.C., Choi, H., Liao, H., 2021. Control of particulate nitrate air pollution in China. *Nat. Geosci.* 14, 389–395.
- Zheng, B., Tong, D., Li, M., Liu, F., Hong, C.P., Geng, G.N., Li, H.Y., Li, X., Peng, L.Q., Qi, J., Yan, L., Zhang, Y.X., Zhao, H.Y., Zheng, Y.X., He, K.B., Zhang, Q., 2018. Trends in China's anthropogenic emissions since 2010 as the consequence of clean air actions. *Atmos. Chem. Phys.* 18, 14095–14111.